J. Math. Biol. (2010) 61:617–647
DOI 10.1007/s00285-009-0314-3

**Mathematical Biology**

# Stochastic modelling of biased cell migration and collagen matrix modification

**Andreas Groh · Alfred K. Louis**

Received: 17 April 2009 / Revised: 9 November 2009 / Published online: 10 December 2009


**Abstract** Matrix dynamics plays a crucial role in several physiological and pathological processes. In this paper we develop a model framework, which describes the temporal fibre network evolution depending on the influence of migrating fibroblasts. The cells are regarded as discrete objects in the plane, whose velocities are determined by a generalised Langevin equation. For its solution we verify existence and uniqueness. The courses of the trajectories are affected by two external impulses, chemotaxis and contact guidance, respectively. The extracellular matrix is described by a continuous vector field which contains both information on density and orientation of the fibrous material. Modelling dynamic interaction between the discrete and the continuum variables is an essential point of this paper. In particular, the smoothing of the fluctuating paths plays a key role. Besides a detailed description of the formulated equations, we also supply the condensed pseudo code of the algorithm. We investigate several examples and present results both from artificial and real data.

**Keywords** Stochastic modelling · Chemotaxis · Contact guidance · Extracellular matrix

**Mathematics Subject Classification (2000)** 92C17 · 92C30 · 92C50 · 60G35

## 1 Introduction

Cell migration is a phenomenon which occurs in many biological processes. There are substantially two kinds of locomotion: swimming and crawling (Bray 2001). The first one is observable in the case of bacteria or ciliata. These microorganisms possess

A. Groh (✉) · A. K. Louis
Fakultät für Mathematik und Informatik, Postfach 151150, 66041 Saarbrücken, Germany
e-mail: groh@num.uni-sb.de

one or several oscillating tails to produce a forward thrust in a liquid medium. In contrast, crawling cells need a substrate, which allows attachments to the cell membrane. These reversible bindings between special ligands and receptors are the premises for conveying forces. In this paper, we concentrate on the second mode of locomotion.

Living cells react in various ways to information from their environment. Typical influences are soluble or fixed molecules, heat, light, an electric potential and others. If a significant translocation towards the source of such an impulse is observable, then this behaviour is called (*positive*) *taxis*. Depending on the mode, a prefix is added, e.g., *chemo*, *photo* or *galvano* (Lo et al. 2000). The term *chemotaxis* represents the preferred motion of a biological cell along a chemical gradient. *Haptotaxis* denotes the unidirectional movement in a adhesion gradient with respect to the surrounding substrate (Carter 1965).

Fibroblasts are eukaryotic cells which can be found in connective tissue. These cells are essential in dermal wound healing because they are responsible for repairing the extracellular matrix (ECM) (Clark 1993). However, in pathological processes, e.g., the *desmoplastic stromal reaction* (DSR), fibroblasts play a key role (Kalluri and Zeisberg 2006). The basic principles of this reaction will be presented later in more detail as their mathematical description is one aim of this paper.

Fibroblasts exhibit both chemotaxis (Postlethwaite et al. 1981) and contact guidance (Friedl and Bröcker 2000; Lo et al. 2000; McCarthy et al. 1996). *Contact guidance* is the bidirectional migration of cells along physical structures of defined shape, e.g. fibre strands (Friedl and Bröcker 2000). Its principle can also be explained, at least on the cellular level, on the basis of movement along a path of preferential adhesion (Carter 1965).

The focus of interest in this paper is fibroblast migration with directional cues via chemotaxis and contact guidance, respectively, and the associated ECM-modification. In literature, only a few relevant mathematical models can be found which contain both features. Naturally, they operate on the cell or tissue level. On the coarsest scale, densities of the involved quantities are described. Based on mechano-chemical considerations, this approach usually leads to systems of coupled nonlinear partial differential equations, often called *taxis-diffusion-reaction problems* (Dale et al. 1997; Dallon and Sherratt 2000; Olsen et al. 1998). On the cell level, Dallon et al. published a series of papers which put emphasis on wound healing (Dallon 2000; Dallon et al. 1999; McDougall et al. 2006). These approaches led to some fundamental ideas of the model introduced in this paper.

In reality it is impossible to predict the pathway of single cells exactly. In cases of taxis-influenced migration, only trends can be forecasted. In a homogeneous medium without external stimuli the trajectories resemble realisations of stochastic processes. In fact, at least with regards to fibroblasts it has been verified that the time-dependent cell velocity for this cell type can be well described by an Ornstein-Uhlenbeck process (Dunn and Brown 1987) which is the solution of the classical Langevin equation (Arnold 1973). This approach has been shown to be appropriate for cells that move according to a random walk, but the velocity equation can be generalised to describe taxis induced by external impulses and contact guidance. A detailed classification into categories of stochastic models which describe biased cell migration, can be found in Ionides et al. (2004). The mentioned mathematical framework has been successfully

adopted to describe biological reactions, especially angiogenesis (Capasso and Morale 2009; Mantzaris et al. 2004; Stokes and Lauffenburger 1991) and the movement of human granulocytes in an electric field (Schienbein and Gruler 1993).

In this paper we interprete fibroblast migration paths as realisations of stochastic processes because in a deterministic approach the observations would not be adequately assessed. We describe the velocity of each cell by a suitable generalised Langevin equation, which incorporates both chemotaxis and contact guidance. The distribution of the soluble attractant is determined by the diffusion equation with appropriate initial and boundary values. The ECM is characterised as a vector field where the Euclidean norm is interpreted as the time-dependent average collagen density in the vicinity of a special point in the domain. Similarly, the normalised vector is regarded as the main direction of the fibrous material. The temporal evolutions of the aforementioned quantities are characterised by ordinary differential equations, where the right hand sides are functions of smoothed versions of the cell trajectories. The mathematical formulation of the stated interaction between the continuum variables, i.e. attractant and collagen on the one hand and the discrete variables which are the single cell positions and velocities, on the other hand, is the principle part of this paper.

This article is organised as follows. In Sect. 2, we briefly outline the biomedical fundamentals of the regarded pathological process. The essential part is Sect. 3, where we describe the mathematical model in detail. Therein, we first summarise the basic assumptions and then introduce the necessary variables to describe the ECM. This is followed by the derivation of the adequate taxis equation and the dynamics of the fibrous material respectively. Afterwards, the concerning interactions between the different types of variables are treated in detail. Section 4 addresses further issues of the numerical implementation and contains the condensed algorithm as pseudo code. In Sect. 5, we illustrate the results of the simulations by considering various scenarios, including real segmentation data. Thereby, we examine the effects of altering some of the key parameters. According to our observations, we suggest that the presented model adequately depicts the regarded biological processes. A discussion of the results and underlying equations, as well as an outlook on future work are presented in Sect. 6. Section 7 serves as an appendix, where we sourced out the proof of existence and uniqueness with regards to the solution of the stochastic differential equation that describes the cell paths.

## 2 Biomedical fundamentals of the desmoplastic stromal reaction

The interaction between tumour cells, stromal cells and ECM plays an important role in cancer progression (Gregoire and Lieubeau 1995; Lubkin and Jackson 2002). The production of abundant connective tissue in cancer is called *desmoplastic stromal reaction* (DSR) and is a hallmark of invasive carcinomas. Many factors exert influence on this complex interaction between the responsible participants of this reaction. As recently stated, the overall effect of altered ECM and the effect of carcinoma-associated fibroblasts on associated phenotypes like angiogenesis, are still poorly understood (Kalluri and Zeisberg 2006).

Tumour cells contain a potent high-molecular-weight chemoattractant for fibroblasts (Gleiber and Schiffmann 1984; van Kempen et al. 2004). Within 11 days, this protein can induce a fibrous tissue mass which is three to five times larger than in controls (Gleiber and Schiffmann 1984). The stroma at the cancer-host interface is produced to a large extent by myofibroblasts and contains various amounts of type I, III, and V collagens, hyaluronic acid, chondroitin sulfate proteoglycan, tenascin-C, and fibronectin (Hauptmann et al. 2003; Kalluri and Zeisberg 2006). Soluble and insoluble forms of collagen I and fibronectin have recently been reported to be capable of inducing remarkable motogenic activity in association with both chemotaxis and haptotaxis (Thibault et al. 2007). Fibronectin, a high molecular weight glycoprotein, allows cells to move through the ECM by connecting cells with collagen fibers (Clark 1993). It binds collagen and certain transmembrane glycoprotein receptors, called integrins. These components facilitate cell movement by mediating cell-matrix adhesion. Integrins may hence be considered responsible for guiding migration along existing fibre strands. Both chemotaxis and contact guidance therefore modulate fibroblast migration on the extracellular matrix.

## 3 The model

### 3.1 Model assumptions and basic definitions

In this study it is presumed, that fibroblasts reply to two independent directional stimuli: chemotaxis (McCarthy et al. 1996) and contact guidance (Even-Ram and Yamada 2005; Friedl and Bröcker 2000; Guido and Tranquillo 1993). Chemotaxis premises the existence of a soluble agent, the chemoattractant, which diffuses in the spatial domain, where sources and possibly sinks can be also located. Contact guidance is mediated through directional impulses due to fibre alignment of the extracellular matrix. The ECM, as part of the connective tissue, may be considered as a biphasic viscolelastic medium (Barocas and Tranquillo 1997) which contains fibrous structures (Kalluri and Zeisberg 2006). The predominant component is collagen, a protein chain which exhibits high tensile strength. The fibroblasts are not only influenced by the matrix, they actively alter the constitution of the fibrous material. This is referred to as *dynamical reciprocity* (Clark 1993). During their migration, the cells dissolve collagen enzymatically via ECM-degrading proteases (Friedl and Bröcker 2000; Kalluri and Zeisberg 2006) and conversely deposit new fibres in the domain (Dallon and Sherratt 1998). Thereby, we follow the approach of Dallon et al. (1999) and assume that the rates of the direction and density changes depend on the already existing collagen and correlate with the cell velocity or to the course of the cell paths (see also Bray 2001; Clark 1993). In Olsen et al. (1998) this hypothesis is referred to as the *flux induced alignment model*.

Mathematically, we introduce two classes of variables: on the one hand, the single cells as individual objects, denoted as *discrete variables*, and on the other hand, the globally defined chemoattractant and the fibrous material, referred to as the *continuum variables* (Dallon 2000). The particular quantities influence each other, so adequate equations need to be enunciated, which depict these interactions. Instead of modelling

each fibre separately, the ECM is characterised as a vector field $\mathbf{f}$, which is both time and space dependent:

$$\mathbf{f} : [0, T] \times \mathbb{R}^d \longrightarrow \mathbb{R}^d.$$

Let $\Omega \subset \mathbb{R}^d$ be the region of interest (ROI). Then for $\mathbf{x} \in \Omega$, the Euclidean norm $\|\mathbf{f}(t, \mathbf{x})\|$ is taken as the average density of the fibrous material at time $t \in [0, T]$. Accordingly, $\mathbf{f}(t, \mathbf{x}) / \|\mathbf{f}(t, \mathbf{x})\|$ is the average direction at $(t, \mathbf{x})$. In an analogous manner, $c(t, \mathbf{x})$ represents the density of the attractant at position $\mathbf{x}$ and time $t$. We shall now describe the cell migration, before the continuum variables $\mathbf{f}$ and $c$ are considered.

### 3.2 Cell paths

Fibroblast $i \in \{1, \ldots, M\}$ is characterised by its position $\mathbf{X}_t^{(i)}$ and velocity $\mathbf{V}_t^{(i)}$ at time $t \in [0, T]$. In this context, the cell is regarded as a point object or a small particle (see Schienbein et al. 1994 for a comprehensive discussion concerning this assumption). The equation for the position of cell $i$ at time $t$ is formally deterministic:

$$d\mathbf{X}_t^{(i)} = \mathbf{V}_t^{(i)} dt. \tag{1}$$

The rate of temporal change in velocity is determined by a generalised Langevin equation. This is a stochastic differential equation (SDE), that comprises a viscous damping term, a noise term and a directional cue $\mathbf{T}_{\text{ext}}^{(i)} = \mathbf{T}_{\text{ext}}^{(i)}\left(t, \mathbf{X}_t^{(i)}, \mathbf{V}_t^{(i)}\right) \in \mathbb{R}^d$. The SDE may be written as

$$d\mathbf{V}_t^{(i)} = \underbrace{-\beta \mathbf{V}_t^{(i)} dt}_{\substack{\text{friction}}} + \underbrace{\mathbf{T}_{\text{ext}}^{(i)} dt}_{\substack{\text{external} \\ \text{stimuli}}} + \underbrace{\alpha d\mathbf{W}_t^{(i)}}_{\substack{\text{random} \\ \text{fluctuations}}}, \tag{2}$$

where $\alpha$ and $\beta$ are positive constants and $\mathbf{W}_t$ is a vectorial standard Wiener process. Equations (1) and (2) can be combined into the system

$$d\begin{bmatrix} \mathbf{X}_t \\ \mathbf{V}_t \end{bmatrix} = \begin{bmatrix} \mathbf{0} & \mathbf{I} \\ \mathbf{0} & -\beta \mathbf{I} \end{bmatrix} \begin{bmatrix} \mathbf{X}_t \\ \mathbf{V}_t \end{bmatrix} dt + \begin{bmatrix} \mathbf{0} \\ \mathbf{T}_{\text{ext}} \end{bmatrix} dt + \begin{bmatrix} \mathbf{0} \\ \alpha \mathbf{I} \end{bmatrix} d\mathbf{W}_t, \tag{3}$$

where the cell index is omitted and $\mathbf{I}$ is the $d \times d$ unit matrix. In the following, we denote by $\langle \cdot, \cdot \rangle$ the standard inner product on $\mathbb{R}^d$. Now let $\mathbf{g}$ be the directional stimulus, e.g. $\mathbf{g} = \nabla c^\top$ for chemotaxis and $\mathbf{g} = \tilde{\mathbf{f}}$, with

$$\tilde{\mathbf{f}}(t, \mathbf{X}_t) = \begin{cases} \mathbf{f}(t, \mathbf{X}_t), & \text{if } \langle \mathbf{f}(t, \mathbf{X}_t), \mathbf{V}_t \rangle \geq 0 \\ -\mathbf{f}(t, \mathbf{X}_t), & \text{else} \end{cases}$$

in the case of contact guidance (Dallon et al. 1999). The last definition expresses that fibres have no orientation, therefore the cell always deflects towards the obtuse angle

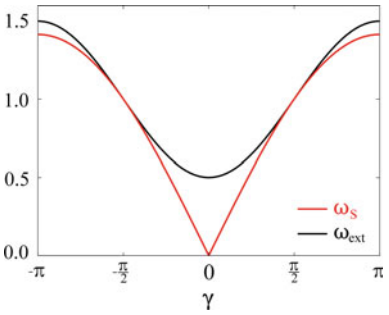


**Fig. 1** Illustration of the weights $\omega_S$ and $\omega_{ext}$ as functions of the enclosed angle $\gamma = \angle(\mathbf{g}, \mathbf{V}_t)$

between $\mathbf{f}$ and $\mathbf{V}_t$. The impulse term is then characterised by

$$\mathbf{T}_{ext} = \mathbf{T}_{ext}(\mathbf{V}_t, \mathbf{g}(t, \mathbf{X}_t)) = \frac{\kappa}{2}\left(1 - \frac{1}{2}\frac{\langle \mathbf{g}, \mathbf{V}_t\rangle}{||\mathbf{g}||\,(||\mathbf{V}_t|| + \varepsilon)}\right)\mathbf{g} \tag{4}$$

for $\mathbf{g} \neq \mathbf{0}$ and a small $\varepsilon > 0$. A brief calculation shows that the limit of $\mathbf{T}_{ext}$ as $\mathbf{g}$ approaches $\mathbf{0}$ is also $\mathbf{0}$. Thus, we have a removable singularity at $\mathbf{g} = \mathbf{0}$ and we set $\mathbf{T}_{ext}(\mathbf{v}, \mathbf{0}) = \mathbf{0}$.

The exposed vector $\mathbf{T}_{ext}$ is an approximation of the chemotaxis term $\mathbf{T}_S$, which was suggested by Stokes and Lauffenburger (1991). More precisely, for $\mathbf{g}, \mathbf{V}_t \neq \mathbf{0}$ and $\phi = \angle(\mathbf{g}, \mathbf{V}_t)$, we have

$$\begin{aligned}
\mathbf{T}_S = \kappa \sin\left|\frac{\phi}{2}\right|\mathbf{g} &= \frac{\kappa}{\sqrt{2}}\sqrt{1 - \frac{\langle \mathbf{g}, \mathbf{V}_t\rangle}{||\mathbf{g}||\,||\mathbf{V}_t||}}\,\mathbf{g} \\
&\approx \frac{\kappa}{\sqrt{2}}\left(1 - \frac{1}{2}\frac{\langle \mathbf{g}, \mathbf{V}_t\rangle}{||\mathbf{g}||\,||\mathbf{V}_t||}\right)\mathbf{g} \\
&\approx \frac{\kappa}{\sqrt{2}}\left(1 - \frac{1}{2}\frac{\langle \mathbf{g}, \mathbf{V}_t\rangle}{||\mathbf{g}||\,(||\mathbf{V}_t|| + \varepsilon)}\right)\mathbf{g} = \mathbf{T}_{ext},
\end{aligned}$$

where primarily a trigonometric identity for the sine is used. The first approximation is the truncation of the binomial series, which is valid since the absolute value of the second summand is less or equal to one according to Cauchy's inequality. The subsequent approximation smooths the term at $\mathbf{V}_t = \mathbf{0}$.

Comparing both coefficients of $\mathbf{T}_S$ and $\mathbf{T}_{ext}$ reveals a different weighting of the force term, i.e. we have $\mathbf{T}_S = \frac{\kappa}{\sqrt{2}}\omega_S\mathbf{g}$ and $\mathbf{T}_{ext} = \frac{\kappa}{\sqrt{2}}\omega_{ext}\mathbf{g}$ with

$$\omega_S = \sqrt{1 - \frac{\langle \mathbf{g}, \mathbf{V}_t\rangle}{||\mathbf{g}||\,||\mathbf{V}_t||}} \quad \text{and} \quad \omega_{ext} = 1 - \frac{1}{2}\frac{\langle \mathbf{g}, \mathbf{V}_t\rangle}{||\mathbf{g}||\,(||\mathbf{V}_t|| + \varepsilon)}. \tag{5}$$

Figure 1 illustrates the graphs of both coefficients for constant $\mathbf{g}/||\mathbf{g}||$ as a function of the enclosed angle between $\mathbf{g}$ and $\mathbf{V}_t$, where we suppose a cell velocity of 10 µm/h and a 'smoothing velocity' of $\varepsilon = 8 \cdot 10^{-3}$ µm/h. The most significant difference is at $\gamma = \angle(\mathbf{g}, \mathbf{V}_t) = 0$, where $\omega_S = 0$ and $\omega_{ext} = 0.5$. This leads to an extension of

the persistence time $P_V$ if the absolute value of $\gamma$ is small. At least for the contact guidance observed by fibroblasts, $P_V$ is reported to be enhanced (Friedl and Bröcker 2000), so this effect is quite convenient.

The results of the numerical simulations for both directional cues $\mathbf{T}_S$ and $\mathbf{T}_{\text{ext}}$ are comparable, but it can be shown that $\mathbf{T}_S$ fails to satisfy the Lipschitz condition with respect to $(\mathbf{X}_t, \mathbf{V}_t)$. This requirement is necessary for standard uniqueness theorems (Øksendal 1998). We did not succeed in finding a verifiable theorem with weaker requirements. If $\mathbf{T}_{\text{ext}}$ obeys the representation in Eq. (4), then the Lipschitz as well as the growth condition for system (3) can be checked. Hence with prescribed initial values, a solution $(\mathbf{X}_t, \mathbf{V}_t)$ exists and is unique. This assertion is formulated as theorem and proven in the appendix. In the following, we briefly verify that $\mathbf{T}_S$ violates the Lipschitz condition where we use proof by contradiction. At first we set $\kappa = 1$ and consider the case of constant force, $\mathbf{g} = \mathbf{e}_1$. We suppose that a positive constant $L$ exists, so that for all $\mathbf{v}_1, \mathbf{v}_2 \neq \mathbf{0}$

$$\|\mathbf{T}_S(\mathbf{v}_1) - \mathbf{T}_S(\mathbf{v}_1)\| = \left|\sin\left|\frac{\phi_1}{2}\right| - \sin\left|\frac{\phi_2}{2}\right|\right| \leq L\,\|\mathbf{v}_1 - \mathbf{v}_2\|\,. \tag{6}$$

Using the representation of the weights in (5), we calculate for $\mathbf{v}_1 = (\varepsilon, \varepsilon)^\top$, $\varepsilon > 0$ and $\mathbf{v}_2 = -\mathbf{v}_1$

$$\|\mathbf{T}_S(\mathbf{v}_1) - \mathbf{T}_S(\mathbf{v}_2)\| = \frac{1}{\sqrt{2}}\left\{\sqrt{1+\frac{1}{\sqrt{2}}} - \sqrt{1-\frac{1}{\sqrt{2}}}\right\} \quad \text{and} \quad \|\mathbf{v}_1 - \mathbf{v}_2\| = 2\sqrt{2}\varepsilon.$$

Inserting this into (6) gives

$$\frac{K}{4} \leq L\varepsilon \quad \text{with} \quad K = \sqrt{1+\frac{1}{\sqrt{2}}} - \sqrt{1-\frac{1}{\sqrt{2}}}.$$

Finally, the choice $\varepsilon = \frac{K}{8L}$ yields the contradiction.

*Nondimensionalisation* In order to run simulations and facilitate the interaction with the continuum variables, it is beneficial to deal with nondimensional quantities. Therefore, we introduce the scaling time unit $u_T$ and length unit $u_L$ and write

$$t = t^* u_T, \quad \mathbf{X}_t = \mathbf{X}^*_{t^*} u_L \quad \text{and} \quad \mathbf{V}_t = \mathbf{V}^*_{t^*}\frac{u_L}{u_T}.$$

For the temporal change in position, we conclude

$$d\mathbf{X}^*_{t^*} = \mathbf{V}^*_{t^*} dt^*$$

and due to $d\mathbf{W}_t = \sqrt{u_T} d\mathbf{W}_{t^*}$, we obtain

$$d\mathbf{V}^*_{t^*} = -\beta^* \mathbf{V}^*_{t^*} dt^* + \mathbf{T}^*_{\text{chemo}} dt^* + \mathbf{T}^*_{\text{cg}} dt^* + \alpha^* d\mathbf{W}_{t^*}$$

with $\beta^* = \beta u_T$ and $\alpha^* = \alpha u_T^{3/2} u_L^{-1}$. The directional impulse terms require a more in-depth study. We start with chemotaxis, pursuing the approach of Stokes and Lauffenburger (1991) and scale the attractant with the maximal concentration $c_0$, i.e. $c = c^* c_0$. This leads to the dimensionless chemical gradient $\nabla_{\mathbf{x}^*} c^*$ with $\nabla_{\mathbf{x}} c = \nabla_{\mathbf{x}^*} c^* c_0 u_L^{-1}$. We finally arrive at the nondimensional chemotaxis term

$$\mathbf{T}^*_{\text{chemo}} = \frac{\kappa^*}{\sqrt{2}} \left( 1 - \frac{1}{2} \frac{\nabla_{\mathbf{x}^*} c^* \mathbf{V}^*_{t^*}}{\|\nabla_{\mathbf{x}^*} c^*\| \left( \left\| \mathbf{V}^*_{t^*} \right\| + \varepsilon^* \right)} \right), \tag{7}$$

where $\varepsilon^* = \varepsilon u_T u_L^{-1}$ and $\kappa^* = \kappa c_0 u_T^2 u_L^{-2}$. Before regarding the contact guidance term, we have to specify the detailed characterisation of the fibre vector field, so we provide the corresponding nondimensionalisation later. For notational simplification, asterisks are omitted hereafter and all variables are dimensionless, if not stated otherwise.

The existence and uniqueness theorem uses a truncated Taylor expansion for the directional impulse and therefore requires smoothness arguments of the force field. This is easy to check for the attractant gradient, because the density distribution is the solution of an appropriate diffusion equation and thus infinitely smooth. Unfortunately, this does not hold for the bi-directional impulse. We capture this topic in the discussion in more detail and utilize the introduced force term for both biases, because the choice seems to be adequate for the purpose of simulation.

### 3.3 The extracellular matrix

The temporal evolution of $\left( \mathbf{X}_t^{(i)}, \mathbf{V}_t^{(i)} \right)$ is a realisation of a stochastic process and thus it is, depending on the weighting of the Wiener process, more or less fluctuating. The new fibres do not follow these paths exactly. Moreover, before the collagen chains are finally deposited in the substratum, they undergo a slight traction which straightens them (Harris et al. 1981). Therefore, the fibres are on one hand associated with a smoothed version $\left( \tilde{\mathbf{X}}_t^{(i)}, \tilde{\mathbf{V}}_t^{(i)} \right)$ of $\left( \mathbf{X}_t^{(i)}, \mathbf{V}_t^{(i)} \right)$ and on the other hand, $\mathbf{f}(t, \mathbf{x})$ is not modified until the cell passed the position $\mathbf{x}$. Thus the temporal delayed information $\left( \tilde{\mathbf{X}}_{t-\tau}^{(i)}, \tilde{\mathbf{V}}_{t-\tau}^{(i)} \right)$ and not the current is taken into account. Thereby, $\tau$ denotes a time lag reflecting the fact that reorientation does not take place before the cell has passed the position (cf. Fig. 2a) (Olsen et al. 1999).

The vector field $\mathbf{f}$ is represented in polar coordinates. The norm $r = ||\mathbf{f}||$ is taken as the mean density and $\boldsymbol{\omega} = \mathbf{f}/||\mathbf{f}||$ as the direction of the fibrous material. In order to specify the temporal evolution of $r$ and $\boldsymbol{\omega}$, let us suppose for the moment that $t$ and $\mathbf{x}$ are fixed. We consider the progress of

$$r(s) = \|\mathbf{f}(t+s, \mathbf{x})\| \quad \text{and} \quad \boldsymbol{\omega}(s) = \frac{\mathbf{f}(t+s, \mathbf{x})}{\|\mathbf{f}(t+s, \mathbf{x})\|}$$

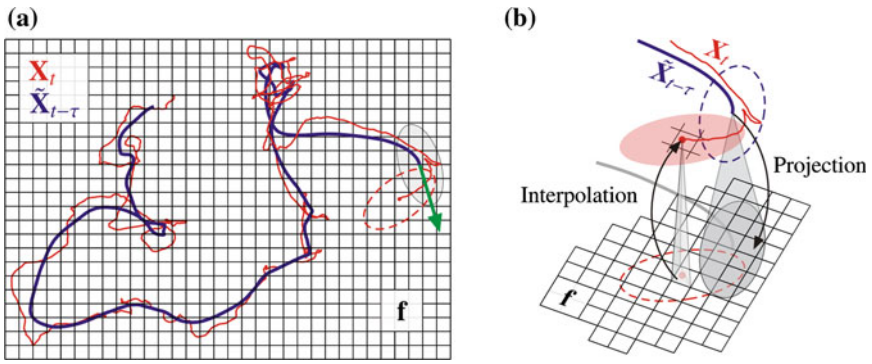


**Fig. 2** Principle of the employed hybrid method. **a** Spatial grid, typical cell trajectory $\mathbf{X}_t$ (*thin line*) and its smoothed, time-lagged version $\tilde{\mathbf{X}}_{t-\tau}$ (*thick line*). The *arrow* denotes $\tilde{\mathbf{V}}_{t-\tau}$. **b** Interaction between the continuum variable **f** and the discrete variable

as functions of $s \geq 0$. Then, the density of the fibrous material evolves according to Dallon et al. (1999)

$$\frac{dr}{ds}(s) = \left(p_f - d_f\, r(s)\right) \sum_{i=1}^{M} w_i(\mathbf{x}), \tag{8}$$

where $p_f$ and $d_f$ are positive constants which represent the production and the decay rate respectively. Differential equation (8) reflects the assumption of a constant production rate and an exponential decay. Obviously, $r_s = p_f/d_f$ is the steady state of the fibre density, in which the complement of cells and ECM allows an equilibrium among various tissue components (Clark 1993).

The scalar functions $w_i \in [0, 1]$ in (8) measure the influence of cell $i$ on the position $\mathbf{x}$. Since this effect is local, every $w_i$ possesses a small support. These functions realise the projection of the fibroblasts information on the continuum variable $\mathbf{f}$ (Fig. 2b). The particular characterisation of the weight functions is carried out later in more detail. At this point, it should just be noted, that the support of $w_i$ is an approximation of the fibroblast's shape. Consequently, if for a time span there are no cells is in the vicinity of point $\mathbf{x}$, then the sum in Eq. (8) vanishes, which results in a constant density. According to the flux induced alignment model, this accounts for the assumption that only fibroblasts alter the fibrous material (Olsen et al. 1998).

Before specifying the rate of change in the fibre direction, we define the *weighted cumulative velocity vector* $\bar{\mathbf{V}}$ at $\mathbf{x} \in \Omega$, which does not depend on $s$. This vector may be considered as a measure of the joint effect, which the fibroblasts exert on the fibrous material at position $\mathbf{x}$. Translated into the current notation, the analogous expression of Dallon et al. (1999) may be written as

$$\bar{\mathbf{V}}_D(\mathbf{x}) = \sum_{i=1}^{M} w_i(\mathbf{x}) \frac{\tilde{\mathbf{V}}_{t-\tau}^{(i)}}{\left\| \tilde{\mathbf{V}}_{t-\tau}^{(i)} \right\|}. \tag{9}$$

This formulation has a major weakness which we elucidate with an example. For this purpose, we consider two vectors $\mathbf{V}^{(1)} = -\mathbf{V}^{(2)}$ with according weight functions

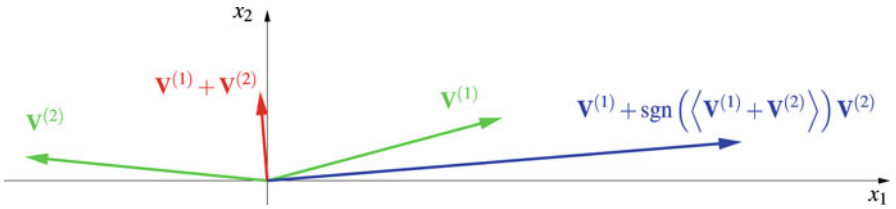


**Fig. 3** Exemplary comparison of both weighted velocity vectors according to (9) and (11), respectively. The sum $\mathbf{V}^{(1)}+\mathbf{V}^{(2)}$ represents a vector being approximately perpendicular to the expected directional cue. Contrary to this, vector $\mathbf{V}^{(1)}+\operatorname{sgn}\left(\left\langle \mathbf{V}^{(1)},\mathbf{V}^{(2)}\right\rangle\right)\mathbf{V}^{(2)}$, determined by (10), mediates the correct alignment impulse for the fibre rotation

$w_1 = w_2$. Inserted in Eq. (9), these vectors sum up to zero, i.e. their joint contribution to the fibrous material vanishes. However, as mentioned above $\pm\tilde{\mathbf{V}}^{(i)}_{t-\tau}$ are equivalent directions concerning fibre alignment, therefore continuing the example, the vectors $\mathbf{V}^{(1)}$ and $\mathbf{V}^{(2)}$ should perform an enlarged fibre rotation in the same direction and not cancel each other (cf. Fig. 3).

Another critical point is the independence of the alignment impulse from the magnitudes of the cell velocities. According to the flux alignment model, the alignment increases both with the number of cells and their speed (Olsen et al. 1998). Therefore, we omit the normalisation in Eq. (9). Additionally in order to prevent cancellations, we have to take the enclosed angles of the smoothed velocity vectors into account. For instance, we postulate that two vectors sum up to (see Fig. 3)

$$\mathbf{S}_v\left(\mathbf{V}^{(1)},\mathbf{V}^{(2)}\right) = w_1\mathbf{V}^{(1)} + \operatorname{sgn}\left(\left\langle \mathbf{V}^{(1)},\mathbf{V}^{(2)}\right\rangle\right) w_2\mathbf{V}^{(2)}. \tag{10}$$

One might think that this strategy can be inductively expanded for more than two velocities, but the example $\mathbf{V}^{(1)} = \mathbf{e}_1$, $\mathbf{V}^{(2)} = \mathbf{e}_2$ and $\mathbf{V}^{(3)} = -\mathbf{e}_1$ reveals that the resulting linear combination is not well-defined because the outcome depends on the summation order. Due to this observation, we define $\bar{\mathbf{V}}$ as a function of the two vectors $\tilde{\mathbf{V}}^{(i_1)}_{t-\tau}$ and $\tilde{\mathbf{V}}^{(i_2)}_{t-\tau}$ that possess maximal weights $w_{i_1}$ and $w_{i_2}$ at position $\mathbf{x}$. If this procedure fails to yield uniqueness, the lengths of the $\tilde{\mathbf{V}}^{(i)}_{t-\tau}$ are additionally taken into account. Since in (11) the magnitudes of the velocities are involved and because of the larger support of the improved weight functions, the turning parameter $\kappa$ is smaller than in the mentioned reference. Finally, we define

$$\begin{aligned}&\bar{\mathbf{V}}\left(t,\mathbf{x},\boldsymbol{\omega}(0),\mathbf{S}_v\left(\tilde{\mathbf{V}}^{(i_1)}_{t-\tau},\tilde{\mathbf{V}}^{(i_2)}_{t-\tau}\right)\right)\\ &\quad= \operatorname{sgn}\left(\left\langle \boldsymbol{\omega}(0),\mathbf{S}_v\left(\tilde{\mathbf{V}}^{(i_1)}_{t-\tau},\tilde{\mathbf{V}}^{(i_2)}_{t-\tau}\right)\right\rangle\right)\mathbf{S}_v\left(\tilde{\mathbf{V}}^{(i_1)}_{t-\tau},\tilde{\mathbf{V}}^{(i_2)}_{t-\tau}\right),\end{aligned} \tag{11}$$

where we have modified the sign function in such a way that $\operatorname{sgn}(0) = 1$. Using some standard algebra, it is easy to verify that the order of $\tilde{\mathbf{V}}^{(i_1)}_{t-\tau}$ and $\tilde{\mathbf{V}}^{(i_2)}_{t-\tau}$ has no influence on $\bar{\mathbf{V}}$, thus this vector is in fact well defined.

Now, let $\theta = \theta(s)$ be the positive angle between $\boldsymbol{\omega}(s)$ and $\bar{\mathbf{V}}$. From (11) it follows that $\theta(0) \in [0, \pi/2]$ and according to the model assumptions, the cells alter the

orientation of the fibrous material in such a way that $\theta$ gets smaller. Analogously to the statement in Dallon et al. (1999), we consider the ordinary differential equation

$$\frac{d\theta}{ds}(s) = -\kappa \left\|\bar{\mathbf{V}}\right\| \sin(\theta(s)), \tag{12}$$

which describes the decay of the enclosed angle as a function of length $\left\|\bar{\mathbf{V}}\right\|$ and the sine of the current angle. We finally define

$$\boldsymbol{\omega}(s) = \mathbf{D}^{\sigma\{\theta(0)-\theta(s)\}}\boldsymbol{\omega}(0),$$

where $\sigma = \operatorname{sgn}\left(\left\langle \mathbf{e}_3, \boldsymbol{\omega}(0) \times \bar{\mathbf{V}}\right\rangle\right)$, which ensures rotation in the correct direction. Thereby, the rotation matrix $\mathbf{D}^{\varphi}$ is defined as usual by

$$\mathbf{D}^{\varphi} = \begin{bmatrix} \cos\varphi & -\sin\varphi \\ \sin\varphi & \cos\varphi \end{bmatrix}. \tag{13}$$

We conclude this subsection with a nondimensionalisation of the equations describing the fibre evolution. As a result of weighted velocity vector already being dimensionless, simply the scaling of the temporal variable $s$ is required in (12)—therefore details are not shown. The density $r$ is scaled with a constant density $r_0$, which leads to

$$\frac{dr^*(s^*)}{ds^*} = \left(p_f^* - d_f^* r^*(s^*)\right) \sum_{i=1}^{M} w_i$$

with $p_f^* = p_f u_T r_0^{-1}$ and $d_f^* = d_f u_T$. Analogously to the chemotaxis term, we characterise the dimensionless contact guidance term and arrive at

$$\mathbf{T}_{cg}^* = \frac{\kappa_{\mathrm{cg}}^*}{\sqrt{2}} \left(1 - \frac{1}{2} \frac{\left\langle \tilde{\mathbf{f}}^*, \mathbf{V}_{t^*}^* \right\rangle}{\|\tilde{\mathbf{f}}^*\| \left(\left\|\mathbf{V}_{t^*}^*\right\| + \varepsilon^*\right)}\right) \tag{14}$$

with $\tilde{\mathbf{f}} = \tilde{\mathbf{f}}^* r_0$ and $\kappa_{\mathrm{cg}}^* = \kappa_{\mathrm{cg}} r_0 u_T^2 u_L^{-1}$. In the following, we omit all asterisks again and deal with dimensionless quantities if not otherwise specified.

*Smoothing of the trajectories* The aim is to construct a smoothed version of the processes $(\mathbf{X}_t, \mathbf{V}_t)$ at time $t - \tau > 0$ for fixed $\tau > 0$. The following considerations are expounded for a scalar signal, i.e. for a bounded sequence $\{y_k\}_{k\in\mathbb{Z}}$. If $y_k$ denotes the sample of a process at discrete time $t_k$, the sequence is also called *time series*. In the terminology of signal processing, a *filter* or *system* is an operator which transforms one signal into another. A particular class are the linear, time-invariant filters. These systems can be written as discrete convolutions with an *impulse response* $h$ (Oppenheim and Schafer 1975), i.e.

$$\tilde{y}_k = (h * y)_k = \sum_{i\in\mathbb{Z}} h_i y_{k-i}.$$

Special impulse responses are *windows* given by

$$h_k = \begin{cases} v_k, & k_l \le k \le k_u \\ 0, & \text{else} \end{cases},$$

where $k_l \le k_u \in \mathbb{Z}$. In this paper we also assume that $h$ satisfies the normalisation condition $\sum v_k = 1$. The *length* of the filter is given by $L = k_u - k_l + 1$. Dependent on the shape of the window, there are a lot of filters established, e.g. *rectangular* (*moving average*, MA), i.e. with constant nonzero entries $v_k = 1/L$ or *triangular* (*Bartlett*) among others. Furthermore, the well-known *Savitzky-Golay smoothing filter* can also be written as convolution with a window.

Contrary to many applications in signal processing, we are interested in filters that flatten sharp peaks. Even with short lengths, this aim is achieved by the usage of the MA system which, in addition, minimises the costs because the smoothed values satisfy the recursive scheme

$$\tilde{y}_k = \tilde{y}_{k-1} + \frac{y_{k-k_l} - y_{k-k_u-1}}{L}. \tag{15}$$

Concerning the time lag, we assume $\tau = j\Delta t$ for a $j \in \mathbb{N}$. This condition can easily be generalised for an arbitrary $\tau$ by the use of linear interpolation between the adjacent filtered values. Regarding the position, the aim is to characterise

$$\tilde{\mathbf{X}}_{t_n - \tau} = \tilde{\mathbf{X}}_{n-j}$$

for given $\mathbf{X}_0, \mathbf{X}_1, \ldots, \mathbf{X}_n$. A centered scheme, i.e. with $k_u = -k_l$, appears reasonable, but $\mathbf{X}_n$ is the latest value, which can be taken into account. If the filter operates only on present and past values, then it is called *causal*. These systems are applicable online, which is a premise of the present application. Here, the principle of causality implies that $k_l = -j$ and $k_u = L - 1 - j$, where $L$ is the specified length. Assuming $n \ge L$, we use (15) for each component with $k = n - j$ to get the smoothed position $\tilde{\mathbf{X}}_{n-j}$. Since convolution is a linear operation, the scheme for the smoothed velocity can be easily calculated via

$$\tilde{\mathbf{V}}_{n-j} = \frac{\tilde{\mathbf{X}}_{n+1-j} - \tilde{\mathbf{X}}_{n+1}}{\Delta t} = \frac{\mathbf{X}_{n+1} - \mathbf{X}_{n+1-L}}{L\Delta t}.$$

*Weight functions* The weight functions $w_i$ in (8) and (11) serve to project the cell information on the spatial domain $\Omega$. As mentioned above, we assume that $w_i(\mathbf{x}) \in [0, 1]$ for all $\mathbf{x} \in \Omega$. Furthermore, the support of $w_i$ should be local and approximate the shape of the fibroblast (Dallon 2000). We choose a prolate spheroid $C$ as cell morphology as this seems to be a good approximation of the spindle-shaped fibroblasts in the ECM (see Fig. 4a) (Friedl and Bröcker 2000). Thereby, the directions of the major axis and the velocity vector $\tilde{\mathbf{V}}_{n-j}$ coincide and $\tilde{\mathbf{X}}_{n-j}$ is the centre of the spheroid (cf. Figs. 2 and 4).

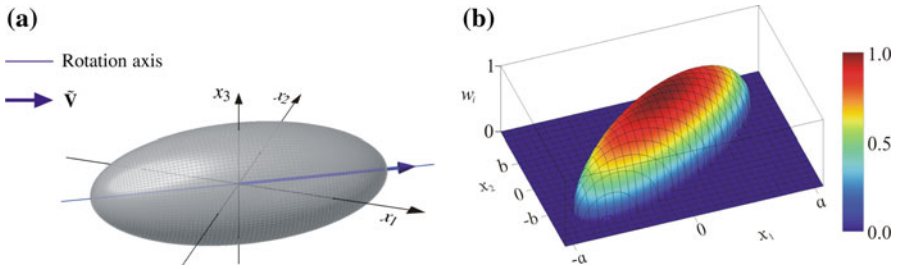


**Fig. 4** Characterisation of the weight function. **a** Spheroid, centered in the origin. **b** Graph of $w_i$

Now, let $\chi_C$ be the characteristic function of the spheroid. Then the value of $w_i$ at $\mathbf{x}$ is the scaled X-ray transform of $\chi_C$ along the $x_3$-axis trough $\mathbf{x}$ (see Fig. 4b). We assume $a$ and $b$ to be the half length of the major and minor axis. Furthermore, we denote by $\gamma$ the angle of $\tilde{\mathbf{V}}_{n-j}$ and define

$$\boldsymbol{\xi} = \mathbf{D}^{-\gamma}\left(\mathbf{x} - \tilde{\mathbf{X}}_{n-j}\right),$$

where $\mathbf{D}$ is a rotation matrix, specified by (13). With $\boldsymbol{\xi} = (\xi_1, \xi_2)^\top \in \mathbb{R}^2$, we finally obtain

$$w_i(\mathbf{x}) = \begin{cases} \sqrt{1 - \left(\frac{\xi_1}{a}\right)^2 - \left(\frac{\xi_2}{b}\right)^2}, & \text{if } \left(\frac{\xi_1}{a}\right)^2 + \left(\frac{\xi_2}{b}\right)^2 \leq 1, \\ 0, & \text{else} \end{cases}$$

which reflects that $w_i(\mathbf{x}) = 1$ if $\mathbf{x}$ is the centre of the spheroid (cf. Figs. 2 and 4). An exemplary graph of $w_i$ is illustrated in Fig. 4b, where $\tilde{\mathbf{X}}_{n-j} = \mathbf{0}$ and $\tilde{\mathbf{V}}_{n-j} = (\cos(\frac{\pi}{6}), \sin(\frac{\pi}{6}))^\top$.

## 4 Numerical implementation

Fundamentally, there are two kinds of variables. On the one hand, the continuum variables $c$ and $\mathbf{f}$ are defined on the whole domain $\Omega \subset \mathbb{R}^2$. On the other hand, there are the fibroblasts regarded as independent entities, which can in principle be located at every position in $\Omega$. Therefore the processes $\left(\mathbf{X}^{(i)}, \mathbf{V}^{(i)}\right)$, $i \in \{1, \ldots, N\}$ are called *discrete variables*. As mentioned above, there is a permanent interaction between the different quantities (Fig. 2). Such systems mixing both types of variables are referred to as *hybrid methods* (Dallon 2000).

For numerical simulations $\Omega$ has to be discretized. For both $c$ and $\mathbf{f}$, we choose a rectangular grid $\Omega_h$ with the same stepsize $h$ in each direction. It follows, that these variables are only defined on fixed lattice points $\mathbf{x_m} \in \Omega_h$, where $\mathbf{m} \in \mathbb{N}^2$ is a multi-index. The influence of the attractant distribution on the cells is unidirectional because the change of agent in the vicinity of the fibroblasts can be neglected. This does not hold for the collagen fibres, because the cells alter their velocities as a consequence of contact guidance and, during their motion, they modify density and orientation of

the fibrous material. From a mathematical viewpoint, we have an alternating cycle of projection and interpolation (see Fig. 2b). The projection of the cell information in (8) and (12) is mediated by the aforementioned weight functions $w_i$, which can also be interpreted as *point spread functions*.

Conversely, we obtain approximations $\mathbf{f}_I(t, \mathbf{X}_t) \approx \mathbf{f}(t, \mathbf{X}_t)$ and $\nabla c_I(t, \mathbf{X}_t) \approx \nabla c(t, \mathbf{X}_t)$ via interpolation. Then, the values $\mathbf{f}_I$ and $\nabla c_I$ can be inserted in (4) to determine the directional cues via chemotaxis and contact guidance, respectively. Thereby, the order of interpolation is chosen to be low because the number of lattice points in the vicinity can be small, e.g. at inner boundaries. In the present application, linear interpolation seems to be adequate, where, if possible, the closest three points are taken as nodes (cf. Fig. 2b). If less adjacent points are available, we utilise the *nearest neighbour* method, i.e. constant approximation in the direction of the absent coordinates.

*Numerical solution of the SDE* The system (3) is nonlinear, autonomous and exhibits additive noise. We apply the Euler-Maruyama (EM) scheme, which yields convergence of order one in this case. The initial values $(\mathbf{X}_0, \mathbf{V}_0)$ are chosen as constants. Furthermore, we assume a fixed stepsize $\Delta t = T/N$ for $N \in \mathbb{N}$, i.e. $t_n = n\Delta t$. The EM method yields a time discrete approximation of the stochastic process, which, for notational simplification, is also called $(\mathbf{X}, \mathbf{V})$. The resulting time series $(\mathbf{X}_n, \mathbf{V}_n)$ satisfies the iterative scheme

$$\mathbf{X}_{n+1} = \mathbf{X}_n + \Delta t \mathbf{V}_n, \tag{16a}$$

$$\mathbf{V}_{n+1} = (1 - \beta\Delta t)\mathbf{V}_n + \Delta t \mathbf{T}_{\text{ext}}(\mathbf{V}_n, \mathbf{g}_I(t_n, \mathbf{X}_n)) + \alpha\Delta\mathbf{W}, \tag{16b}$$

for $n = 0, 1, \ldots, N-1$, where we have written $(\mathbf{X}_n, \mathbf{V}_n) = \left(\mathbf{X}_{t_n}, \mathbf{V}_{t_n}\right)$. Thereby, the increment of the Wiener process $\Delta\mathbf{W}$ is normally distributed with mean $\mathbf{0}$ and covariance matrix $\sqrt{\Delta t}\,\mathbf{I}$.

*Diffusion* According to the model assumptions, the tumour acts as the source of the chemoattractant. In fact, there might be several molecules on which the fibroblasts reply with positive taxis, e.g. small peptides or collagen fragments (McCarthy et al. 1996) and other factors (Gleiber and Schiffmann 1984). However, we unify them to just one chemical attractant. This agent diffuses freely in the ECM, so we presume that its concentration $c = c(t, \mathbf{x})$ solves the diffusion equation. Normally, there are immersed fixed structures in the ROI. For example, we can encounter tumours, healthy or necrotic tissue and possibly other solid objects like bones. The boundaries of the biological shapes are represented by polygons that posses more or less complex geometries. To circumvent inner boundaries in the diffusion domain, we make the simplifying assumption that the solute also diffuses within the structures, however with very small diffusion coefficient. Let $\chi_T$ and $\chi_S$ denote the characteristic functions of the tumour tissue and the remaining structures, respectively. Then, we declare the space-dependent diffusion coefficient $\mu$ by

$$\mu(\mathbf{x}) = \begin{cases} \mu_1, & \text{if } \chi_T(\mathbf{x}) + \chi_S(\mathbf{x}) = 1 \\ \mu_2, & \text{else} \end{cases}, \tag{17}$$

where $0 < \mu_1 \ll \mu_2$. At the current state of research, no information about solute distributions in the regarded tissues are available, thus, we suggest the initial condition (IC)

$$c(0, \mathbf{x}) = c_0 \chi_T(\mathbf{x})$$

with a constant concentration $c_0$. It cannot be excluded, that tumours intersect the boundaries of the ROI, so we conduct an artificial enlargement of the domain and deal with homogeneous Dirichlet data. For the sake of simplicity, the expanded area is also denoted by $\Omega$, hence, the initial-boundary value problem is summarised as follows:

$$\text{(PDE)} \quad c_t(t, \mathbf{x}) = \operatorname{div}\left(\mu(\mathbf{x}) \operatorname{grad} c(t, \mathbf{x})\right), \quad \mathbf{x} \in \Omega, \ t \in [0, T], \tag{18a}$$

$$\text{(IC)} \quad c_0 c(0, \mathbf{x}) = \chi_T(\mathbf{x}), \quad \mathbf{x} \in \Omega, \tag{18b}$$

$$\text{(BC)} \quad c(t, \mathbf{x}) = 0, \quad \mathbf{x} \in \partial\Omega. \tag{18c}$$

The nondimensionalisation of the diffusion equation is straightforward. We choose a characteristic temporal unit $u_T$ and a spatial unit $u_L$ and define

$$t = t^* u_T, \quad \mathbf{x} = \mathbf{x}^* u_L, \quad c(t, \mathbf{x}) = c^*(t^*, \mathbf{x}^*), \quad \mu(\mathbf{x}) = \mu^*(\mathbf{x}^*)\mu_0.$$

By using the chain rule for partial derivatives, we arrive at

$$c^*_{t^*} = \mu_0^* \operatorname{div}\left(\mu^*(\mathbf{x}^*) \operatorname{grad} c^*(t^*, \mathbf{x}^*)\right) \tag{19}$$

with $\mu_0^* = \mu_0 u_T u_L^{-2}$. The scaling of corresponding initial and boundary conditions is straightforward, so details are not shown. Analogously to the aforementioned subsections, we also omit the asterisks for notational simplification and deal with nondimensional quantities.

For the numerical solution of (19), we use the Peaceman–Rachford algorithm (Strikwerda 1989). This is a semi-implicit ADI (Alternating Direction Implicit) method which is based on the Crank-Nicolson scheme.

*Permeability of the immersed structures and the domain boundaries* The ROI is just a part of the examined histological slice, so the ECM normally exceeds the edges of $\Omega$. Consequently, some fibroblasts traverse the boundary $\partial\Omega$ during the simulation. Such a cell is then removed from the numerical experiment and, in return, a new one is randomly inserted into the extracellular matrix. This strategy avoids an unnatural depletion of fibroblasts in the domain.

The fibroblasts migrate solely in the ECM and they cannot infiltrate solid tissues. Since these structures are immersed in the ROI, it is possible that the cells hit such a barrier. Therefore, the cells alter their locomotion and an algorithmic treatment of this fact has to be taken into account. Algorithms for collision detection between particles and polygons are well-known. The crucial point is not the mathematical handling but the computational costs. If an intersection of the trajectory and a structure is detected, i.e. points of the line segment $\mathbf{X}_n + \lambda \Delta t \mathbf{V}_n$, $\lambda \in (0, 1]$ lie inside a circumscribing polygon, we assume that the fibroblast is deflected in an acute angle to its current direction. This means that the cell slides along the edge. At the same time, the new,

rotated velocity $\mathbf{V}_n$, which is now parallel to the encountered polygon segment, is reduced with a retarding factor $\delta \in (0, 1)$.

Obviously, when a cell enters a corner which encloses an acute angle, it is possible, that it iterates the vertex in an infinite loop. In order to avoid this incident, we suggest that if more than three collisions per time step arise, the velocity vector is turned around by $\pi$, giving the cell the possibility to leave the impasse.

*Pseudo code* For a better readability, we omit the $n$th point in time $t_n$ and insert the according subindex instead, i.e. $c_n(\mathbf{x_m}) = c(t_n, \mathbf{x_m})$ and $\mathbf{f}_n(\mathbf{x_m}) = \mathbf{f}(t_n, \mathbf{x_m})$, respectively. Furthermore, we apply the Euler scheme to the ODEs (8) and (12). The achieved order of convergence is one, therefore it is identical to the order of the EM method applied to the SDE (3).

```
Input:  (X_0^(i), V_0^(i)) for all i ∈ {1, ..., M}
        f_0(x_m) and ∇c_0(x_m) for all x_m ∈ Ω_h

for n = 0 : N − 1
    for i = 1 : M
        interpolate f_n(X_n^(i)) and ∇c_n(X_n^(i))
        compute (X_{n+1}^(i), V_{n+1}^(i))
    end
    if n ≥ j
        compute (X̃_{n−j}^(i), Ṽ_{n−j}^(i)) for all i ∈ {1, ..., M}
        for x_m ∈ Ω_h
            r_{n+1}(x_m) = r_n(x_m) + Δt (p_f − d_f r_n(x_m)) Σ_{i=1}^{M} w_i(x_m)
            Δθ_n(x_m) = κ Δt ||V̄|| sin(θ_n(x_m))
            ω_{n+1}(x_m) = D^{σ Δθ_n(x_m)} ω_n(x_m)
            f_{n+1}(x_m) = r_{n+1}(x_m) ω_{n+1}(x_m)
            compute ∇c_{n+1}(x_m)
        end
    end
end
```

## 5 Results

At first, we apply the algorithm to a simple test-scenario, where two circular structures are immersed in the rectangular domain $\Omega$. In Fig. 5, the left one represents the carcinoma, the right one acts merely as a solid barrier for the migrating cells. The next batch of numerical experiments uses real segmentation data. Before expounding the specific settings of the two geometries, we first outline the common features.

In both cases we take a spatial stepsize of $h = 10\,\mu\text{m}$ in each direction. For every $i$, we assume the support of $w_i$ to be an ellipse with half major axis $a = 30\,\mu\text{m}$ and half minor axis $b = 10\,\mu\text{m}$, reflecting the spindle-shaped geometry of the fibroblasts. To

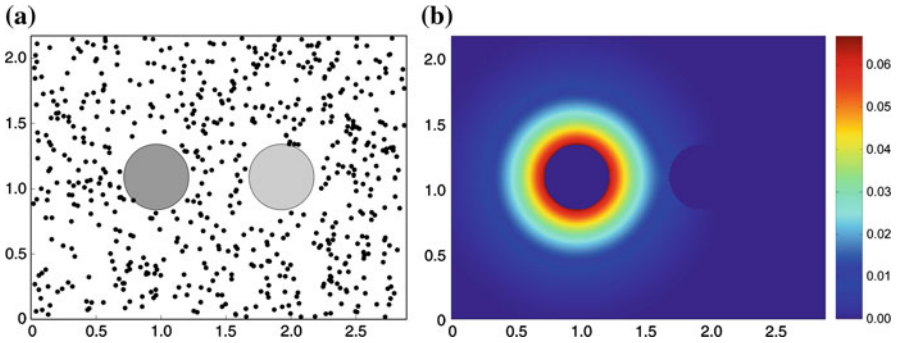


**Fig. 5** Initial settings of the computational experiments for the artificial geometry. The dots in **a** solely reflect the positions and not the cell shapes. **a** Initial cell distribution. **b** Fixed attractant density

run the simulations, we have to solve the nondimensional equations that describe the evolutions of the concerning quantities. Thereby, we choose the characteristic scaling units as in Dallon et al. (1999), i.e. we set $u_T = 1$ h and $u_L = 10$ μm. The temporal stepsize in the simulation is $\Delta t = 2^{-3}$, which corresponds to 7.5 minutes. In this study, compared with the weight functions in the aforementioned citation, the support of $w_i$ is larger, so we take the slightly extended time lag $\tau = 3\Delta t$. The moving average filter has total length $L = 24$ with $k_l = -3$, that means the filter is causal, as required.

In order to incorporate chemotaxis, we numerically solve the accordant nondimensional initial-boundary problem of the system (18), where we scaled the diffusion domain in such a way that it is congruent with $\Omega$ and adopt the according grid. The dimensionless diffusion coefficients in (17) are $\mu_1 = 0.01$ and $\mu_2 = 1$. For the sake of simplicity, the resulting attractant density after 500 timesteps to the stepsize $\Delta t = 10^{-4}$ is taken as a fixed concentration in the simulations. The corresponding gradient is then numerically calculated by the central difference quotient.

The individual initial migration angle is randomly chosen from $[0, 2\pi]$, the starting magnitude of speed ranges in the physiological meaningful interval of values between 0 and 67 μm/h. Furthermore, we set $\beta = 0.8\ \mathrm{h}^{-1}$ and $\alpha = 10\ \mu\mathrm{m\,h}^{-3/2}$ in (2). The nondimensional intensities for chemotaxis and contact guidance in (7) and (14) are chosen to $\kappa_{\mathrm{chemo}} = 1{,}000$ and $\kappa_{\mathrm{cg}} = 15$, respectively. Another non-physical parameter is the speed scaling factor for which we fixed randomly $\delta = 0.6$.

The collagen density evolution is governed by $p_f = 0.064$ and $d_f = 0.044$ in (8). Both these parameters originate from Dallon et al. (1999), but we used 0.1 as scaling factor. This strategy is caused by the fact that the original values yield the steady state after a short time span. This originates predominantly from the improved weight functions, exhibiting a larger support in the direction of prolongated cell axis. The scaling factor is identical for both $p_f$ and $d_f$, because therewith the absolute value of the steady state $r_s$ remains the same. For most of the simulations in this paper, the turning rate of the mean fibre direction in (12) is set to $\kappa = 0.1$.

To show the effects of each external impulse, we consider the situation with no taxis and either chemotaxis or contact guidance. Finally both these directional cues are taken into account. For every numerical experiment, the fibre density $||\mathbf{f}||$ and the

smoothed cell trajectories are shown. The last mentioned quantity can be interpreted, in a broader sense, as the pathways of the fibres.

Since we visualise realisations of stochastic processes, we always use the same seed state for the random number generator, which allows a better comparability.

### 5.1 Artificial geometry

This simple scenario shows two circular structures in the rectangular domain $\Omega = 2.89 \times 2.18\ \text{mm}^2$. The left one, filled with dark grey, is considered to be the attractant-emitting tumour (see Fig. 5a). The adjacent disk represents healthy tissue and acts as control structure. There are $M = 601$ cells uniformly distributed over the ECM, which corresponds to a cell density of 100 cells per $\text{mm}^2$.

If the cells are not influenced by any directional bias, their velocities are realisations of the well-known Ornstein-Uhlenbeck process (Kloeden and Platen 1999). Integration with respect to the time variable yields the corresponding paths, which are smoothed by the aforementioned moving average filter in every time step (see Fig. 6a). In this case, we have $\mathrm{E}[\mathbf{X}_t] = \mathbf{X}_0$ and therefore a minor tendency to cover large distances from the starting position. This in turn, may lead to a strong anisotropy of the fibre density and the absence of any alignment (see Fig. 7a).

If the cell behaviour is influenced by chemotaxis, then we observe a preferred migration towards the attractant producing disk. In regions where the gradient nearly vanishes, e.g. in the right part of $\Omega$, chemotaxis is almost not detectable (see Fig. 6b). The pattern changes entirely if contact guidance acts on the migration of the fibroblasts. Compared with the previous experiments, the common translocation is significantly enlarged. Furthermore, the collagen density is more uniformly distributed over $\Omega$ (Fig. 7c). The increased contact guidance along existing fibre material leads to a preferred migration on already pursued paths. As a result, there arises fibre bundling in the whole domain, which increases with the magnitude of the contact guidance rate. The rise of fibre bundles can be seen on both density representation (Fig. 7c) and illustration Fig. 6c showing the smoothed trajectories.

Obviously, $r_s = p_f/d_f = 16/11$ is the steady state of the fibre density. In both cases, where chemotaxis is involved, the value of $r_s$ is nearly attained. However, in the absence of contact guidance we have a dense collagen capsule around the tumour representing disk (see Fig. 7b). This is not the case if contact guidance affects the migratory behaviour of the fibroblasts. Indeed, the fibre density in the tumour vicinity is enhanced but a capsule is not detectable (cf. Fig. 7d). In reality, the phenomenon of a dense collagen capsule that encompasses tumour tissue, would exert great influence on the pathogenesis of the desmoplastic stromal reaction.

### 5.2 Artificial geometry with pre-existing fibres

So far, the ECM was assumed to be initially void, which is not the case in real tissues. In order to demonstrate the effect of pre-existing fibrous material, we create a simple test scenario, where two regions are assumed to have a constant collagen density of $0.1 r_s$. The location and the particular directions as well as the initial density of the

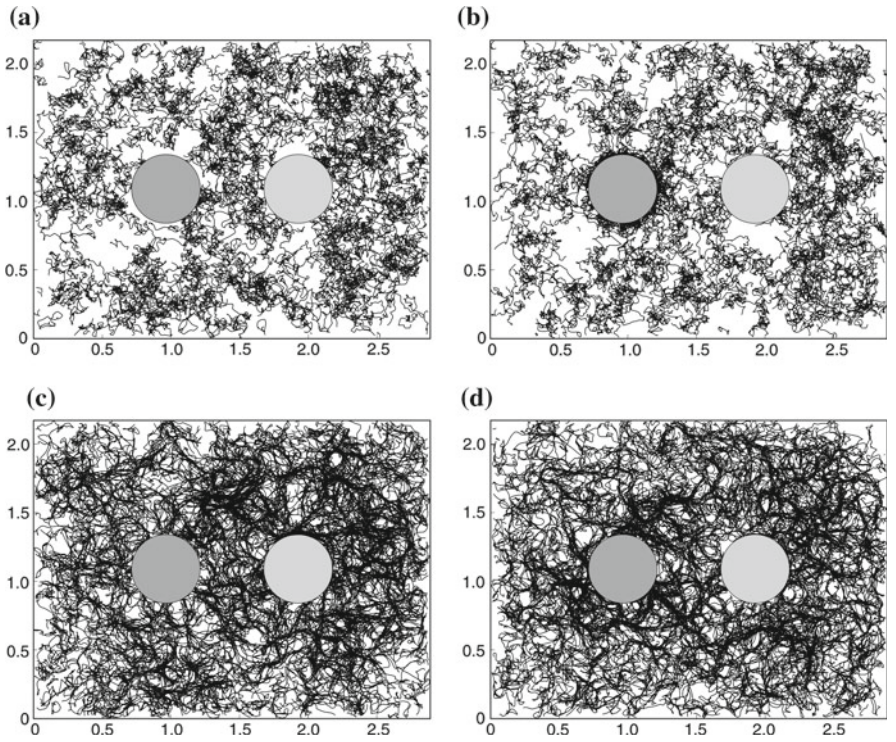


**Fig. 6** Smoothed versions of the cell trajectories. For better illustration, only every second path is displayed. **a** No directional bias acts on the migratory behaviour of the fibroblasts. **b** Chemotaxis leads to a preferred migration towards the attractant source. Contact guidance is neglected. **c** The fibroblasts react with contact guidance on aligned fibrous material. The chemical agent has no influence on the cells. **d** Both chemotaxis and contact guidance are considered to act as directional cues for migrating cells

collagen fibres are indicated in Fig. 8. Furthermore, the prescribed setup is appropriate to study the impact of the parameters $p_f$, $d_f$ and $\kappa$. The former are responsible for the density evolution, the latter characterises the turning rate of $\mathbf{f}$ towards the cumulative velocity vector $\bar{\mathbf{V}}$. For better accentuation of the parameter variations, we neglect chemotaxis in the present experiments.

We observe that the predefined fibre region can be recognised in the graphical representation of the simulation results (esp. in the Fig. 9a and b). Thereby, contact guidance stimulates the fibroblasts to follow pre-existing traces, resulting in predominant parallel migratory paths. As expected, the tendency to alter the primary directions increases with the magnitude of the turning parameter. Thus, if $\kappa$ is small then the initial directions are retained and the incoming cells receive persistent acceleration parallel to $\mathbf{f}$, while they simultaneously increase $\|\mathbf{f}\|$ along their trails. This again provides positive feedback for subsequent fibroblasts, which prefer to follow the existing dense fibre strands via contact guidance. This can be seen in Fig. 9c and d, where the fibre rotation is facilitated. In both these illustrations, the initial setting is difficult to recognise. As mentioned above, we use a scaled version of the original parameters $p_f$ and $d_f$ adopted from Dallon et al. (1999). Thereby, we choose the same factor $c_r$

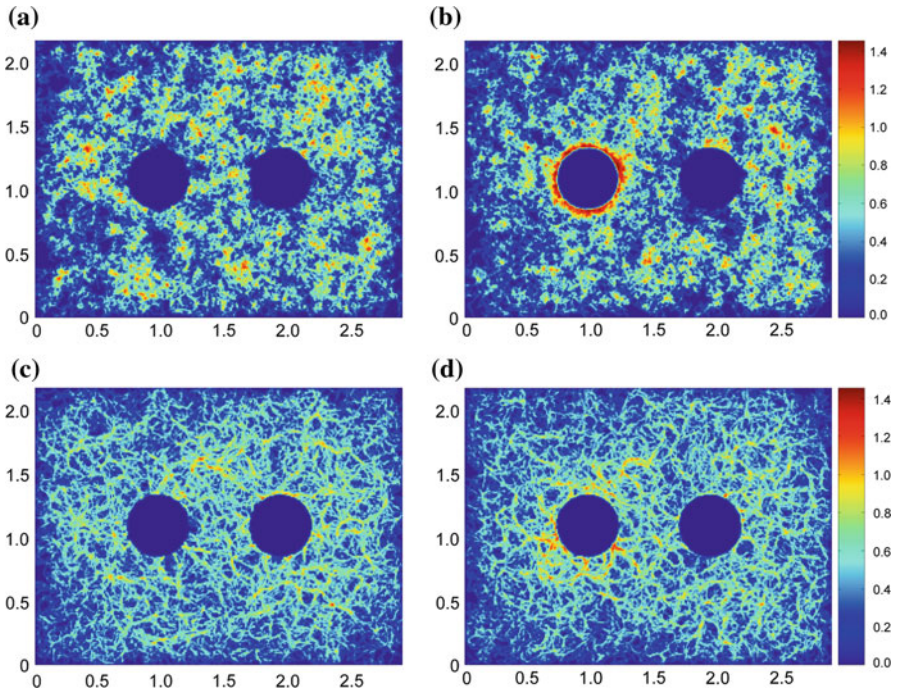


**Fig. 7** Resulting collagen density at the end of the simulations with the artificial scenario. **a** No directional bias acts on the migratory behaviour of the fibroblasts. **b** Chemotaxis leads to a preferred migration towards the attractant source. Contact guidance is neglected. **c** The fibroblasts react with contact guidance on aligned fibrous material. The chemical agent has no influence on the cells. **d** Both chemotaxis and contact guidance are considered as directional cues

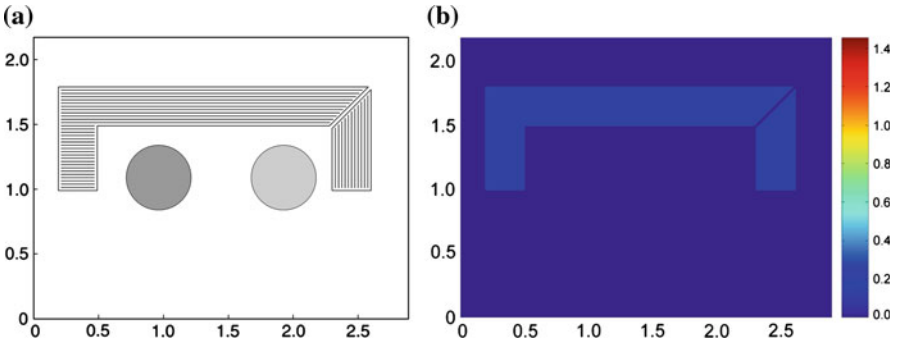


**Fig. 8** Illustration of the input regarding the artificial scenario with a pre-existing fibre vector field. **a** Initial fibre vector field. **b** Initial collagen density

for both values in order to retain the steady state $r_s = p_f/d_f$. The influence of the production and decay rate on the collagen evolution can easily be seen in Fig. 9, where the overall density is significantly enhanced by the doubling of the scaling parameter. This phenomenon is expected with regard to the underlying differential equation (8), for which we henceforth assume the sum of the weights to be constant. Without loss

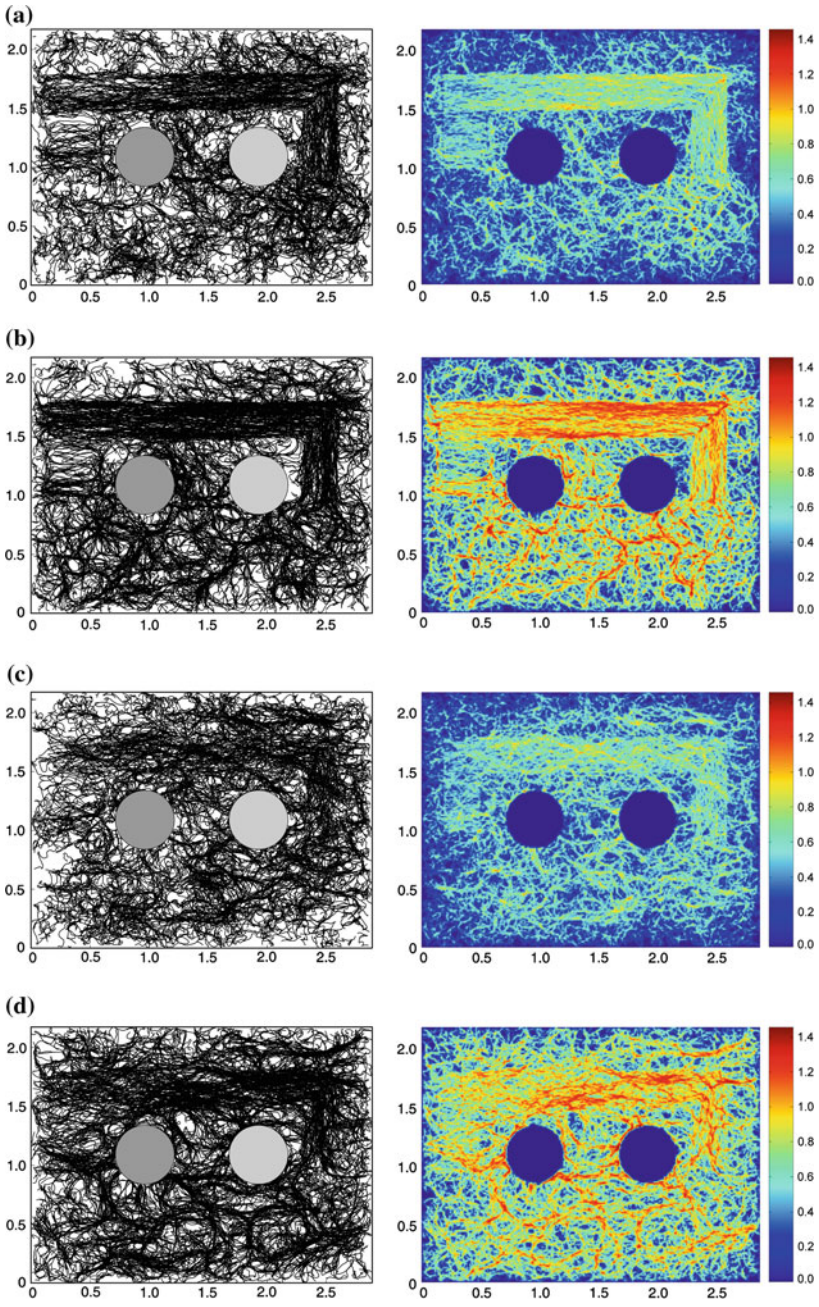


**Fig. 9** Simulation results with pre-existing fibres in the domain. Except for $\kappa$ and the scaling factor $c_r$ of $p_f$ and $d_f$, we have used the same parameters as in Subsect. 5.1. The *left column* shows every second smoothed cell trajectory, the *right column* illustrates the fibre density $r = \|\mathbf{f}\|$. **a** Parameters: $\kappa = 0.1$, $c_r = 0.1$. **b** Parameters: $\kappa = 0.1$, $c_r = 0.2$. **c** Parameters: $\kappa = 0.5$, $c_r = 0.1$. **d** Parameters: $\kappa = 0.5$, $c_r = 0.2$

of generality, we set $\sum w_i = 1$ since the value of the sum does not influence the qualitative predictions. Therewith, it is easy to verify that for a fixed point in $\Omega$,

$$r(t) = r_s - (r_s - r_0)e^{-d_f t}$$

is the solution of the ordinary differential equation (8), where $r_0$ denotes the initial density. Thus, the density increase accelerates with the magnitude of $d_f$.

### 5.3 Histological segmentation data

Anonymised samples of moderately differentiated squamous cell carcinoma of the lung and their surrounding mesenchyme were included in the present study. The tissues were recruited from the regular diagnostic pool of the year 2004 (Saarland University, Department of Pathology, Homburg Saar Campus, Germany), fixed in 4% buffered formaldehyde, embedded in paraffin-wax and subsequently stained with hematoxylin and eosin (H&E). Digital images of the scenarios were manually segmented and histomorphologically classified with the help of the prototypical software named *SeViSe* (Landes et al. 2006).

Since in this paper, we have put emphasis on the mathematical features of the suggested model, we use neither varying histological slices and present biomedical implications, nor do we discuss other topics concerning real data. Instead we leave these fruitful issues for further studies.

The regarded part of the exemplary histological slice (Fig. 10a) shows a characteristical phenotype of the desmoplastic stromal reaction. The accordant segmentation result is displayed in Fig. 10c. If not otherwise stated, we use the same parameters for the simulations as before. Consequently, we have $M = 233$ cells in the domain, which has an estimated extent of $\Omega = 2.04 \times 1.53\,\mathrm{mm}^2$. In order to demonstrate the impact of both directional cues, we firstly choose $\kappa_{\mathrm{chemo}}$ and $\kappa_{\mathrm{cg}}$ as above (first row of Fig. 11) and then reduce these parameters (second row).

Regarding the second column in Fig. 11, it can be observed, that the maximum collagen density is nearly reached in both experiments. However, with regards to the second simulation, it disperses more homogeneously than expected. Similarly, the tendency of generating collagen bundles is reduced with decreased $\kappa_{\mathrm{cg}}$.

## 6 Discussion

In this paper, we have developed a new stochastic model that describes fibre alignment in the extracellular matrix due to the influence of migrating fibroblasts. The innovation originates from the combination and progression of two known approaches, where both were modified with regard to the current problem.

The starting point is the modelling of single cells as functionally discrete entities and the characterisation of their positions and velocities. The most appropriate approach seems to be the modelling of cell speed by a generalised Langevin equation, since cell trajectories are reproduced in a lifelike manner (Dunn and Brown 1987). The characterisation of collagen is also a crucial point. In reality, extracellular matrix

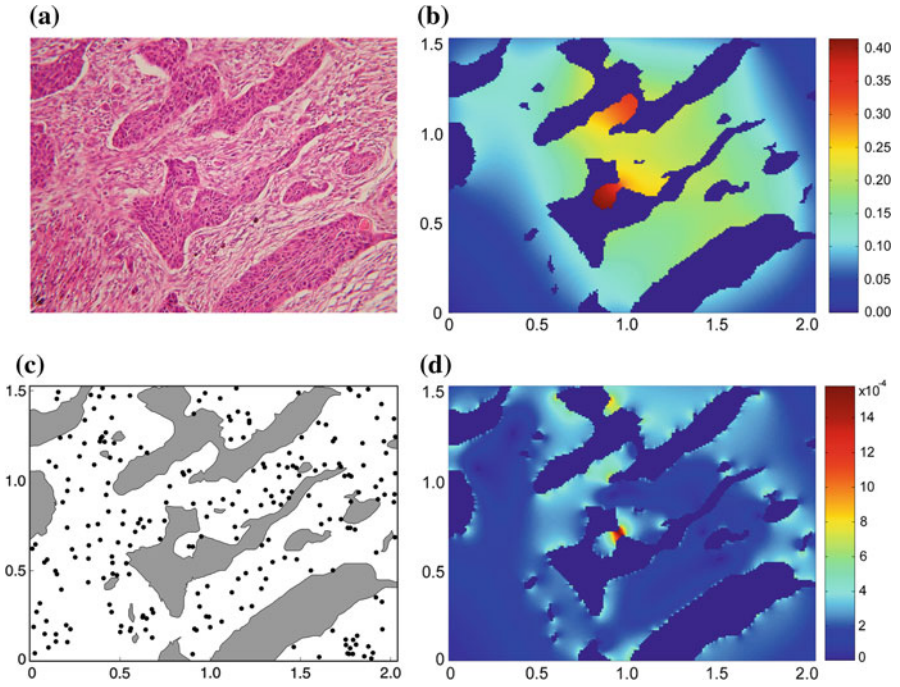


**Fig. 10** Illustration of the input regarding the real histological data. **a** Detail of the histological slice. **b** Attractant density distribution. **c** Segmentation data and initial positions of the fibroblasts. **d** Norm of the attractant gradient

contains a vast number of different sized fibres which, in addition, influence each other mechanically. From a mathematical viewpoint, modelling the specified dynamics is certainly possible, but the computational costs forbid this strategy. Thus, the characterisation as a vector field offers several advantages: on the one hand, the interpretation is straightforward and the complexity can be monitored. On the other hand, the employed impulse term that characterises contact guidance can easily be specified via interpolation.

There are several models which depict directional cues in the velocity equation of the form (2) (Capasso and Morale 2009; Hadeler et al. 2004; Ionides 2001; Mantzaris et al. 2004; Schienbein et al. 1994), especially in the case of chemo- and galvanotaxis. The utilised taxis term $\mathbf{T}_{\text{chemo}}$ is an enhancement of a known ansatz, which adequately depicts biased fibroblast migration (Stokes and Lauffenburger 1991) towards the source of the chemoattractant. Thereby, we have modified the sine factor of the external impulse in such a way, that existence and uniqueness of the stochastic differential equation system for chemotaxis and other unidirectional cues can be verified (see appendix). As mentioned above, the requirements of the existence and uniqueness theorem are naturally fulfilled for chemotaxis because the corresponding attractant distribution is the solution of an appropriate diffusion equation and thus infinitely smooth. For other unidirectional impulses, e.g. galvanotaxis or phototaxis, the smoothness condition of the fields are also presumed to be verifiable in concrete applications. Problems

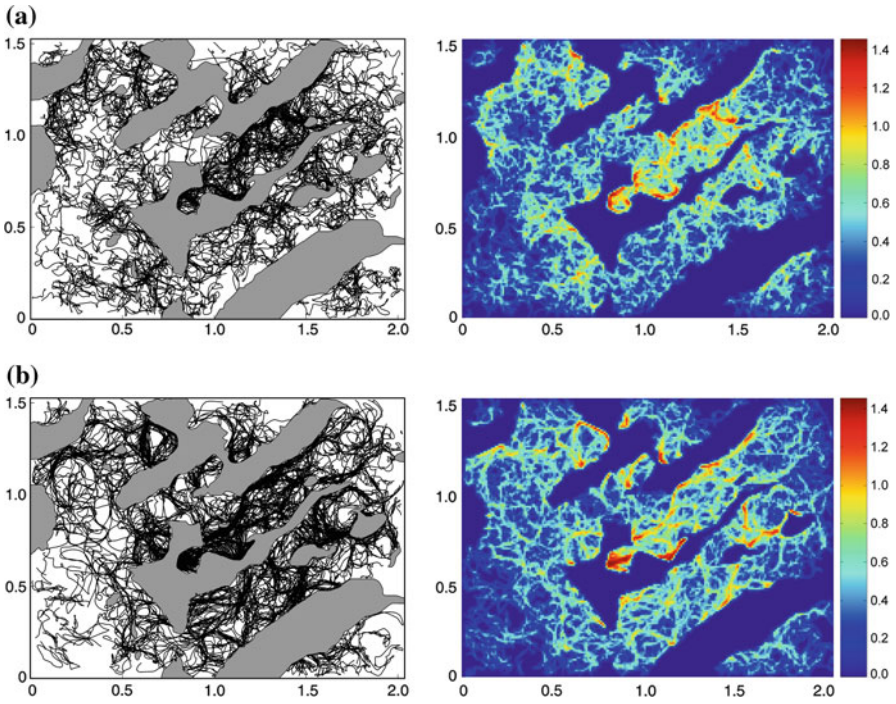


**Fig. 11** Smoothed trajectories (*left column*) and density plots (*right column*) based on real tissue geometries. **a** Parameters: $\kappa_{\text{chemo}} = 500$, $\kappa_{\text{cg}} = 10$. **b** Parameters: $\kappa_{\text{chemo}} = 1,000$, $\kappa_{\text{cg}} = 20$

arise if the force term mediates bi-directional movement like in the case of contact guidance. The situation $\langle \mathbf{g}, \mathbf{V}_t \rangle = 0$, i.e. where the directional cue changes its sign and the cells migrate randomly in either of the opposite directions is crucial. We have not overcome this difficulties yet, so we leave it as an open question for future research.

The modelling of cell migration in real scenarios requires the consideration of immersed solid structures such as compact tissues, bones, blood vessels and so on. Naturally, moving cells hit these impermeable structures during their motion and an algorithmic treatment of these incidents has to be formulated in order to run computational simulations. We propose a deflection in the acute angle to the current direction, parallel to the boundary combined with a simultaneous reduction of the speed. While this ad-hoc modification of the velocity vector seems reasonable for cells as point objects, it dramatically alters the character of the underlying stochastic process. Even with regards to the classical Langevin equation, the presence of immersed complex boundaries implies the pathwise uniqueness of a solution to be extremely hard to verify and perhaps not feasible. So at the current state of research we have no option but to leave its treatment as an open question.

In Subsect. 5.2, we showed that the progression of the simulation depends not only on the model parameters, but also strongly on the initial fibre distribution. According to current knowledge, there are no computer simulations which start with segmentation data of real histological slices, even less with real fibre alignment information.

Methods to remedy this deficiency are in preparation, however the attempts are bidirectional. On the one hand the effort is to find an adequate method that realises the projection of segmented fibre information on the initial vector field. On the other hand, it seems to be feasible to employ image analysis routines to gain morphological information of fibre distributions in digital images of histological slices. Amongst others, a Fourier filtering method either of the masked digitised image of the histological slice or segmentation data of fibres appears to be promising (Chaudhuri et al. 1987).

In the presented form, the model is limited to the two-dimensional case. A generalisation towards three dimensions is straightforward for the Langevin equation which characterises the cell velocity. Unfortunately, this does not hold true for the fibre dynamics. To eradicate this flaw, suitable approaches are in preparation and will be published in an upcoming paper. Another deficiency of the model in its introduced form is the disregarding of cell-cell contacts. It is well-known that the resulting interactions (Chen et al. 2004) in combination with possible shape-changes (Wells et al. 1999) exert influence on cell dispersion, but the integration of either topic would require a completely modified modelling approach. In literature, several papers addressed these topics, e.g. Dickinson and Tranquillo (1993) considers stochastic fluctuations in the cell membrane or Palsson (2001) covers pure deterministic mechanics arising in the case of cell collisions. Yet all these approaches deal with spatial and temporal scales which are much smaller than the ones in this paper. The incorporation of these phenomena on the cellular or molecular level in order to develop a more realistic model is a challenging topic for future research. A first, naive idea might be the modification of the weight functions $w_i$, since they are currently fixed for all cells and depend neither on time, cell speed, nor on the environment. An according generalisation of the model seems to be possible, but in practice this is very difficult to cover, not because of the additional computational costs, but due to the algorithmic treatment of the underlying physical and physiological processes. Since the main goal of this paper is the presentation of the basic model, we have not explored this concept here.

In this first approach of modelling the desmoplastic stromal reaction, we have not distinguished between several molecules reported to induce chemotaxis with regard to fibroblast migration. Accordingly, we have made some strong simplifications concerning the diffusion domain and chose a diffusion coefficient $\mu$ without biomedical substantiation. This has been due to the fact that the aim is merely to compute an exemplary distribution that is related to the complex geometry of the real histological data. The computation of more realistic concentrations for particular chemoattractants would have required not only their correct diffusion rates, but also the information regarding the 3D geometry of the underlying tissue assays, because the existence of inner boundaries affects the diffusion process strongly. Due to the irregularity of the immersed solid structures and outer boundaries, we believe that adaptive techniques are required, as well as the consideration of local sources. This stems from the fact that inflammation cells in the vicinity of the tumours also produce chemoattractants. This in return, would of course imply the modelling of these cell types.

The detailed evaluation of the model is very complex and can only partially be carried out. The employed impulse term in the generalised Langevin equation (2) is an approximation of a known and validated ansatz (Ionides 2001; Stokes and Lauffenburger 1991). As already outlined in Subsect. 3.2, the utilisation of $\mathbf{T}_{\text{ext}}$ results in

an enhanced persistence time. Ionides et al. (2004) (see also Ionides 2001) provide techniques that allow parametric estimation for the generalised Langevin speed equation describing unidirectional migration in a constant external field. This application, which uses cell tracking information, is exemplarily applied to the translocation of human keratinocytes affected by galvanotaxis, however it also possesses the potential to deal with other fields. For instance, successful attempts to create stationary linear attractant gradients can be found (Fisher et al. 1989; Zicha et al. 1991) as well as other methods to gain long-lasting spatially continuous distributions (Knapp et al. 1999). Thus, comparable in vivo investigations of fibroblasts migration would potentially help to determine adequate parameters and allow a rigorous evaluation of the chemotactic migration model. In addition, there are also basic approaches to study contact guidance (Amyot et al. 2008; Guido and Tranquillo 1993), but the methodical handling is reported to be exceedingly difficult.

Similarly, the evaluation of collagen fibre dynamics and the corresponding parameter estimation is a challenging project. Indeed, the parameters regulating the evolution of the fibre density, $p_f$ and $d_f$, as well as the turning rate $\kappa$ are provided in literature (Dallon et al. 1999) and employed in several subsequent publications without modification (Dallon 2000; Dallon et al. 2000; McDougall et al. 2006), but unfortunately without a precise reference. Instead, it is merely stated that these values stem from experimental data (Dallon et al. 1999). Similarly, the factor for non-dimensionalisation of the protein density is not substantiated. All that is mentioned is its scaling is between 0 and 1.5 (Dallon et al. 2000). Thus, we are not able to expound the attainment of those underlying biological values and adopt the particular parameters in such a way that the steady state of the fibre density remains the same. Furthermore, the turning parameter $\kappa$ had to be scaled down, because of the augmented right hand side of (12), the elongated weight functions and the modification of the weighted cumulative velocity vector. The validation of the concerning approach itself is also not completely performed in the aforementioned papers because of the enormous methodical problems. Thereby, the problem generally starts with the acquirement of appropriate fibre alignment measurements as a function of time. Since such data generation requires the fixation and cutting of the tissue, it is impossible to achieve the required time series from patients in vivo. In order to eradicate this flaw, there are attempts to prepare gels with oriented collagen alignment (Girton et al. 1999; Guido and Tranquillo 1993). Suitable in vitro experiments, combined with cell tracking methods could possibly help to bridge the gap, but at the current state of research, this issue has to be left as an open problem.

As a concluding remark, we state that despite the remaining research work, the model seems adequate to simulate biased cell migration and the simultaneous fibre alignment. Furthermore, we emphasise that the presented concept can be easily adapted to describe other physiological or pathological processes, like wound healing or angiogenesis.

**Acknowledgments** The authors would like to thank Priv.-Doz. Dr. med. Mathias Wagner (Saarland University, Department of Pathology) for providing the classified segmentation data.

## Appendix

**Theorem 1** *Let* $\mathbf{g} = \mathbf{g}(t, \mathbf{x})$ *be a bounded two-dimensional function on* $[0, T] \times \Omega$ *without zeros, where* $T > 0$ *and* $\Omega \subset \mathbb{R}^2$. *Furthermore, let the Jacobian* $\mathbf{J_g}(\mathbf{x})$ *be bounded for all* $t$ *and* $\mathbf{x}$. *Then, for each constant* $(\mathbf{X}_0, \mathbf{V}_0)$, *there exists a pathwise unique strong solution of the stochastic initial value problem* (3).

*Proof* We verify the requirement of a standard existence and uniqueness theorem, e.g. Theorem 4.5.3 in Kloeden and Platen (1999). We set $\mathbf{y} = (\mathbf{x}^\top, \mathbf{v}^\top)^\top \in \mathbb{R}^4$ and obtain from (3) the drift vector

$$\mathbf{a}(t, \mathbf{y}) = \begin{bmatrix} \mathbf{v} \\ -\beta\mathbf{v} + \mathbf{T}_{\text{ext}}(\mathbf{v}, \mathbf{g}(t, \mathbf{x})) \end{bmatrix} \tag{20}$$

and the constant diffusion matrix

$$\mathbf{b}(t, \mathbf{y}) = \begin{bmatrix} \mathbf{0} & \mathbf{0} \\ \mathbf{0} & \alpha\mathbf{I} \end{bmatrix}. \tag{21}$$

Since the initial values are assumed to be constant, we have to check three conditions. In the following, it is sufficient to consider $\mathbf{a}$, because $\mathbf{b}$ is a constant matrix and the particular requirements are trivially fulfilled. Without loss of generality, we assume $\|.\|$ to be the Euclidean and $\|.\|_{\text{F}}$ the Frobenius norm.

I. *Measurability*. The function $\mathbf{a}$ is continuous and hence measurable.
II. *Lipschitz condition*. We have to verify that for all $\mathbf{y}_1, \mathbf{y}_2 \in \mathbb{R}^4$ there exists a $K_1 > 0$ with

$$\|\mathbf{a}(t, \mathbf{y}_1) - \mathbf{a}(t, \mathbf{y}_2)\| \leq K_1 \|\mathbf{y}_1 - \mathbf{y}_2\|.$$

At first the triangle inequality yields

$$\|\mathbf{a}(t, \mathbf{y}_1) - \mathbf{a}(t, \mathbf{y}_2)\| \leq (1+\beta) \|\mathbf{v}_1 - \mathbf{v}_2\| + \|\mathbf{T}_{\text{ext}}(\mathbf{v}_1, \mathbf{g}(t, \mathbf{x}_1)) - \mathbf{T}_{\text{ext}}(\mathbf{v}_2, \mathbf{g}(t, \mathbf{x}_2))\|.$$

For better readability, we omit the time-variable, and once more with the triangle inequality we assess

$$\|\mathbf{T}_{\text{ext}}(\mathbf{v}_1, \mathbf{g}(t, \mathbf{x}_1)) - \mathbf{T}_{\text{ext}}(\mathbf{v}_2, \mathbf{g}(t, \mathbf{x}_2))\| \leq \frac{\kappa}{\sqrt{2}} \|\mathbf{g}(\mathbf{x}_1) - \mathbf{g}(\mathbf{x}_2)\| + \frac{\kappa}{2\sqrt{2}} T_1$$

with

$$T_1 = \left\| \frac{\langle \mathbf{g}(\mathbf{x}_2), \mathbf{v}_2 \rangle}{\|\mathbf{g}(\mathbf{x}_2)\| \, (\|\mathbf{v}_2\| + \varepsilon)} \mathbf{g}(\mathbf{x}_2) - \frac{\langle \mathbf{g}(\mathbf{x}_1), \mathbf{v}_1 \rangle}{\|\mathbf{g}(\mathbf{x}_1)\| \, (\|\mathbf{v}_1\| + \varepsilon)} \mathbf{g}(\mathbf{x}_1) \right\|.$$

Taylor's theorem asserts that there exists a $\lambda \in [0, 1]$ with

$$\mathbf{g}(\mathbf{x}_1) = \mathbf{g}(\mathbf{x}_2) + \mathbf{J_g}(\mathbf{x}_2 + \lambda(\mathbf{x}_1 - \mathbf{x}_2))(\mathbf{x}_1 - \mathbf{x}_2).$$

By assumption, the norm of the Jacobian is bounded, i.e. there exists a constant $c_1 > 0$ with

$$\|\mathbf{g}(\mathbf{x}_1) - \mathbf{g}(\mathbf{x}_2)\| \leq c_1 \frac{\sqrt{2}}{\kappa} \|\mathbf{x}_1 - \mathbf{x}_2\| .$$

Further, the triangular inequality yields $T_1 \leq T_2 + T_3$, where

$$T_2 = \left\| \left\langle \frac{\mathbf{g}(\mathbf{x}_2)}{||\mathbf{g}(\mathbf{x}_2)||}, \left( \frac{\mathbf{v}_2}{||\mathbf{v}_2|| + \varepsilon} - \frac{\mathbf{v}_1}{||\mathbf{v}_1|| + \varepsilon} \right) \right\rangle \mathbf{g}(\mathbf{x}_2) \right\|$$

and

$$T_3 = \left\| \mathbf{g}(\mathbf{x}_2) \left\langle \frac{\mathbf{g}(\mathbf{x}_2)}{||\mathbf{g}(\mathbf{x}_2)||}, \frac{\mathbf{v}_1}{||\mathbf{v}_1|| + \varepsilon} \right\rangle - \mathbf{g}(\mathbf{x}_1) \left\langle \frac{\mathbf{g}(\mathbf{x}_1)}{||\mathbf{g}(\mathbf{x}_1)||}, \frac{\mathbf{v}_1}{||\mathbf{v}_1|| + \varepsilon} \right\rangle \right\| .$$

We state that the factor $\|\mathbf{g}(\mathbf{x}_2)\|$ is bounded by a positive constant $c_2$, thus the Cauchy-Schwarz inequality implies

$$T_2 \leq c_2 \left\| \frac{\mathbf{v}_2}{\|\mathbf{v}_2\| + \varepsilon} - \frac{\mathbf{v}_1}{\|\mathbf{v}_1\| + \varepsilon} \right\| .$$

Finally, repeated applications of standard algebra and estimations show that

$$T_2 \leq \frac{2c_2}{\varepsilon} \|\mathbf{v}_2 - \mathbf{v}_1\| .$$

For the term $T_3$, we conclude that

$$\begin{aligned}
T_3 &\leq \left\| \frac{\mathbf{g}(\mathbf{x}_2)\mathbf{g}(\mathbf{x}_2)^\top}{||\mathbf{g}(\mathbf{x}_2)||} - \frac{\mathbf{g}(\mathbf{x}_1)\mathbf{g}(\mathbf{x}_1)^\top}{||\mathbf{g}(\mathbf{x}_1)||} \right\|_{\mathrm{F}} \frac{\|\mathbf{v}_1\|}{||\mathbf{v}_1|| + \varepsilon} \\
&= \left\| \frac{\{\mathbf{g}(\mathbf{x}_2) - \mathbf{g}(\mathbf{x}_1) + \mathbf{g}(\mathbf{x}_1)\}\, \mathbf{g}(\mathbf{x}_2)^\top}{||\mathbf{g}(\mathbf{x}_2)||} - \frac{\mathbf{g}(\mathbf{x}_1)\left\{\mathbf{g}(\mathbf{x}_1)^\top - \mathbf{g}(\mathbf{x}_2)^\top + \mathbf{g}(\mathbf{x}_2)^\top\right\}}{||\mathbf{g}(\mathbf{x}_1)||} \right\|_{\mathrm{F}} \\
&\leq \left\| \frac{\{\mathbf{g}(\mathbf{x}_2) - \mathbf{g}(\mathbf{x}_1)\}\, \mathbf{g}(\mathbf{x}_2)^\top}{||\mathbf{g}(\mathbf{x}_2)||} - \frac{\mathbf{g}(\mathbf{x}_1)\, \{\mathbf{g}(\mathbf{x}_1) - \mathbf{g}(\mathbf{x}_2)\}^\top}{||\mathbf{g}(\mathbf{x}_1)||} \right\|_{\mathrm{F}} \\
&\quad + \left\| \left( \frac{1}{||\mathbf{g}(\mathbf{x}_2)||} - \frac{1}{||\mathbf{g}(\mathbf{x}_1)||} \right) \mathbf{g}(\mathbf{x}_1)\mathbf{g}(\mathbf{x}_2)^\top \right\|_{\mathrm{F}} \\
&\leq \|\mathbf{g}(\mathbf{x}_2) - \mathbf{g}(\mathbf{x}_1)\| + \|\mathbf{g}(\mathbf{x}_2) - \mathbf{g}(\mathbf{x}_1)\| + \left| \frac{1}{||\mathbf{g}(\mathbf{x}_2)||} - \frac{1}{||\mathbf{g}(\mathbf{x}_1)||} \right| \|\mathbf{g}(\mathbf{x}_1)\|\ \|\mathbf{g}(\mathbf{x}_2)\| \\
&= 2\,\|\mathbf{g}(\mathbf{x}_2) - \mathbf{g}(\mathbf{x}_1)\| + |\,\|\mathbf{g}(\mathbf{x}_1)\| - \|\mathbf{g}(\mathbf{x}_2)\|\,| \\
&\leq 3\,\|\mathbf{g}(\mathbf{x}_2) - \mathbf{g}(\mathbf{x}_1)\| \\
&\leq \frac{3\sqrt{2}c_1}{\kappa} \|\mathbf{x}_1 - \mathbf{x}_2\| .
\end{aligned}$$

In summary, we arrive at

$$\|\mathbf{a}(t,\mathbf{y}_1)-\mathbf{a}(t,\mathbf{y}_2)\| \le \frac{K}{\sqrt{2}}\left(\|\mathbf{x}_1-\mathbf{x}_2\|+\|\mathbf{v}_1-\mathbf{v}_2\|\right) \le K\,\|\mathbf{y}_1-\mathbf{y}_2\|$$

with

$$K_1 = \max\left\{\frac{5c_1}{\sqrt{2}}\,,\ \frac{\kappa c_2}{\varepsilon}+\sqrt{2}(1+\beta)\right\},$$

so the required Lipschitz condition is indeed fulfilled.

III. *Linear growth bound*. We have to verify the existence of a constant $K_2 > 0$ with

$$\|\mathbf{a}(t,\mathbf{y})\|^2 \le K_2^2\left(1+\|\mathbf{y}\|^2\right).$$

For the drift vector, we get

$$\|\mathbf{a}(t,\mathbf{y})\|^2 \le \|\mathbf{v}\|^2 + 2\beta^2\,\|\mathbf{v}\|^2 + 2\,\|\mathbf{T}_{\text{ext}}(\mathbf{v},\mathbf{g}(t,\mathbf{x}))\|^2.$$

As mentioned above, $\|\mathbf{g}\|$ is dominated by $c_2$, thus we obtain

$$\begin{aligned}\|\mathbf{T}_{\text{ext}}(\mathbf{v},\mathbf{g}(t,\mathbf{x}))\|^2 &\le \kappa^2\left(1+\frac{|\langle\mathbf{g},\mathbf{v}\rangle|^2}{2\,\|\mathbf{g}\|^2\,(\|\mathbf{v}\|+\varepsilon)^2}\right)c_2^2\\ &\le \kappa^2\left(1+\frac{\|\mathbf{v}\|^2}{2(\|\mathbf{v}\|+\varepsilon)^2}\right)c_2^2 \le \frac{3}{2}\kappa^2 c_2^2.\end{aligned}$$

Finally, we conclude

$$\|\mathbf{a}(t,\mathbf{y})\|^2 \le K_2^2\left(1+\|\mathbf{v}\|^2\right) \le K^2\left(1+\|\mathbf{y}\|^2\right)$$

with $K_2 = \max\left\{\sqrt{1+2\beta^2},\sqrt{3}\kappa c_2\right\}$. Therewith, the requirements of the existence theorem are fulfilled and the stated result follows. □

## References

Amyot F, Small A, Boukari H, Sackett D, Elliott J, McDaniel D, Plant A, Gandjbakhche A (2008) Thin films of oriented collagen fibrils for cell motility studies. J Biomed Mater Res Part B Appl Biomater 86(2):438–443

Arnold L (1973) Stochastische differentialgleichungen, 1st edn. R. Oldenbourg, München, Wien

Barocas VH, Tranquillo RT (1997) An anisotropic biphasic theory of tissue-equivalent mechanics: the interplay among cell traction, fibrillar network deformation, fibril alignment, and cell contact guidance. J Biomech Eng 119(2):137–145

Bray D (2001) Cell movements: from molecules to motility, 2nd edn. Garland, New York

Capasso V, Morale D (2009) Stochastic modelling of tumour-induced angiogenesis. J Math Biol 58: 219–233

Carter S (1965) Principles of cell motility: the direction of cell movement and cancer invasion. Nature 208(5016):1183–1187
Chaudhuri S, Nguyen H, Rangayyan RM, Walsh S, Frank CB (1987) A Fourier domain directional filtering method for analysis of collagen alignment in ligaments. IEEE Trans Biomed Eng 34(7):509–518
Chen CS, Tan J, Tien J (2004) Mechanotransduction at cell-matrix and cell-cell contacts. Ann Rev Biomed Eng 6(1):275–302
Clark RAF (1993) Biology of dermal wound repair. Dermatol Clin 11:647–666
Dale PD, Sherratt JA, Maini PK (1997) Role of fibroblast migration in collagen fiber formation during fetal and adult dermal wound healing. Bull Math Biol 59:1077–1100
Dallon JC (2000) Numerical aspects of discrete and continuum hybrid models in cell biology. Appl Numer Math 32:137–159
Dallon JC, Sherratt JA (1998) A mathematical model for fibroblast and collagen orientation. Bull Math Biol 60(1):101–129
Dallon JC, Sherratt JA (2000) A mathematical model for spatially varying extracellular matrix alignment. SIAM J Appl Math 61(2):506–527
Dallon JC, Sherratt JA, Maini PK (1999) Mathematical modelling of extracellular matrix dynamics using discrete cells: fibre orientation and tissue regeneration. J Theor Biol 199:449–471
Dallon JC, Sherratt JA, Maini PK, Ferguson M (2000) Biological implications of a discrete mathematical model for collagen deposition and alignment in dermal wound repair. IMA J Math Med Biol 17:379–393
Dickinson RB, Tranquillo RT (1993) A stochastic model for adhesion-mediated cell random motility and haptotaxis. J Math Biol 31:563–600
Dunn GA, Brown AF (1987) A unified approach to analysing cell motility. J Cell Sci Suppl 8:81–102
Even-Ram S, Yamada KM (2005) Cell migration in 3d matrix. Curr Opin Cell Biol 17(5):524–532
Fisher PR, Merkl R, Gerisch G (1989) Quantitative analysis of cell motility and chemotaxis in Dictyostelium discoideum by using an image processing system and a novel chemotaxis chamber providing stationary chemical gradients. J Cell Biol 108(3):973–984
Friedl P, Bröcker EB (2000) The biology of cell locomotion within three-dimensional extracellular matrix. Cell Mol Life Sci 57(1):41–61
Girton TS, Dubey N, Tranquillo RT (1999) Magnetic-induced alignment of collagen fibrils in tissue equivalents. In: Tissue engineering methods and protocols, no. 18 in methods in molecular Medicine, 1st edn., chap. 1. Materials. Humana Press, Totowa
Gleiber WE, Schiffmann E (1984) Identification of a chemoattractant for fibroblasts produced by human breast carcinoma cell lines. Cancer Res 44(8):3398–3402
Gregoire M, Lieubeau B (1995) The role of fibroblasts in tumor behavior. Cancer Metastasis Rev 14(4): 339–350
Guido S, Tranquillo RT (1993) A methodology for the systematic and quantitative study of cell contact guidance in oriented collagen gels. Correlation of fibroblast orientation and gel birefringence. J Cell Sci 105(2):317–331
Hadeler KP, Hillen T, Lutscher F (2004) The Langevin or Kramers approach to biological modeling. Math Models Methods Appl Sci 14(10):1561–1583
Harris AK, Stopak D, Wild P (1981) Fibroblast traction as a mechanism for collagen morphogenesis. Nature 290:249–251
Hauptmann S, Siegert A, Berger S, Denkert C, Köbel M, Ott S, Siri A, Borsi L (2003) Regulation of cell growth and the expression of extracellular matrix proteins in colorectal adenocarcinoma: a fibroblast-tumor cell coculture model to study tumor-host interactions in vitro. Eur J Cell Biol 82(1):1–8
Ionides EL (2001) Statistical analysis of cell motion. Ph.D. thesis, University of California, Berkley
Ionides EL, Fang KS, Isseroff RR, Oster GF (2004) Stochastic models of cell motion and taxis. J Math Biol 48:23–37
Kalluri R, Zeisberg M (2006) Fibroblasts in cancer. Nat Rev Cancer 6(5):392–401
Kloeden PE, Platen E (1999) Numerical solution of stochastic differential equations, 3 edn. No. 23 in applications of mathematics, stochastic modelling and applied probability. Springer, Berlin, Heidelberg
Knapp DM, Helou EF, Tranquillo RT (1999) A fibrin or collagen gel assay for tissue cell chemotaxis: assessment of fibroblast chemotaxis to grgdsp. Exp Cell Res 247(2):543–553
Landes CA, Weichert F, Philipp, Helga F, Wagner M (2006) Evaluation of two 3D virtual computer reconstructions for comparison of cleft lip and palate to normal fetal microanatomy. The anatomical record part A: discoveries in molecular, cellular, and evolutionary biology, vol 288.

Wiley, New York, pp 248–262. http://www3.interscience.wiley.com/journal/112394892/abstract?CRETRY=1&SRETRY=0

Lo CM, Wang HB, Dembo M, Wang YL (2000) Cell movement Is guided by the rigidity of the substrate. Biophys J 79:144–152

Lubkin SR, Jackson TL (2002) Multiphase mechanics of capsule formation in tumors. J Biomech Eng 124:237–243

Mantzaris NV, Webb S, Othmer HG (2004) Mathematical modelling of tumor-induced angiogenesis. J Math Biol 49(2):111–187

McCarthy JB, Vachhani B, Iida J (1996) Cell adhesion to collagenous matrices. Pept Sci 40(4):371–381

McDougall S, Dallon JC, Sherratt JA, Maini PK (2006) Fibroblast migration and collagen deposition during dermal wound healing: mathematical modelling and clinical implications. Philos Trans R Soc A Math Phys Eng Sci 364(1843):1385–1405

Øksendal B (1998) Stochastic differential equations, 5th edn. Universitext. Springer, Berlin

Olsen L, Maini PK, Sherratt JA, Dallon J (1999) Mathematical modelling of anisotropy in fibrous connective tissue. Math Biosci 158(2):145–170

Olsen L, Maini PK, Sherratt JA, Marchant B (1998) Simple modelling of extracellular matrix alignment in dermal wound healing i. cell flux induced alignment. Comput Math Methods Med 1:175–192

Oppenheim AV, Schafer RW (1975) Digital signalprocessing. Prentice Hall, Englewood Cliffs

Palsson E (2001) A three-dimensional model of cell movement in multicellular systems. Future Gener Comput Syst 17(7):835–852

Postlethwaite AE, Keski-Oja J, Balian G, Kang AH (1981) Induction of fibroblast chemotaxis by fibronectin. Localization of the chemotactic region to a 140,000-molecular weight non-gelatin-binding fragment. J Exp Med 153:494–499

Schienbein M, Franke K, Gruler H (1994) Random walk and directed movement: comparison between inert particles and self- organized molecular machines. Phys Rev 49(6):5462–5471

Schienbein M, Gruler H (1993) Langevin equation, fokker-planck equation and cell migration. Bull Math Biol 55(3):585–608

Stokes CL, Lauffenburger DA (1991) Analysis of the roles of microvessel endothelial cell random motility and chemotaxis in angiogenesis. J Theor Biol 152:377–403

Stokes CL, Lauffenburger DA (1991) Migration of individual microvessel endothelial cells: stochastic model and parameter measurement. J Cell Sci 99:419–430

Strikwerda JC (1989) Finite difference schemes and partial differential equations. Chapman & Hall/CRC, Boca Raton

Thibault MM, Hoemann CD, Buschmann MD (2007) Fibronectin, vitronectin, and collagen I induce chemotaxis and haptotaxis of human and rabbit mesenchymal stem cells in a standardized transmembrane assay. Stem Cells Dev 16:489–502

van Kempen LC, Rijntjes J, Claes A, Blokx WA, Gerritsen MJP, van Muijen DJRGN (2004) Type I collagen synthesis parallels the conversion of keratinocytic intraepidermal neoplasia to cutaneous squamous cell carcinoma. J Pathol 204(3):333–339

Wells A, Ware MF, Allen FD, Lauffenburger DA (1999) Shaping up for shipping out: PLC$\gamma$ signaling of morphology changes in EGF-stimulated fibroblast migration. Cell Motil Cytoskelet 44(4):227–233

Zicha D, Dunn GA, Brown AF (1991) A new direct-viewing chemotaxis chamber. J Cell Sci 99(4):769–775